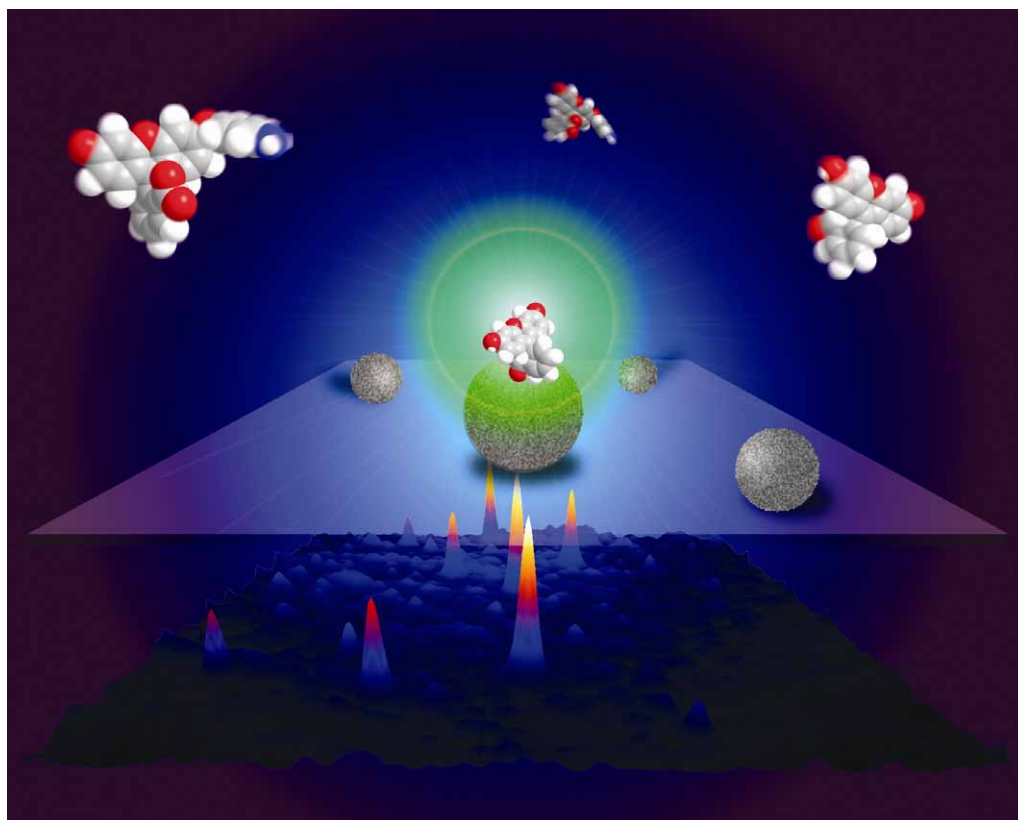# Chem Soc Rev

This article was published as part of the

In-situ characterization of heterogeneous catalysts themed issue

Guest editor Bert M. Weckhuysen

Monitoring surface metal oxide catalytic active sites with Raman spectroscopy†

Israel E. Wachs* and Charles A. Roberts

The molecular aspect of the Raman vibrational selection rules allows for the molecular structural and reactivity determinations of metal oxide catalytic active sites in all types of oxide catalyst systems (supported metal oxides, zeolites, layered hydroxides, polyoxometalates (POMs), bulk pure metal oxides, bulk mixed oxides and mixed oxide solid solutions). The molecular structural and reactivity determinations of metal oxide catalytic active sites are greatly facilitated by the use of isotopically labeled molecules. The ability of Raman spectroscopy to (1) operate in all phases (liquid, solid, gas and their mixtures), (2) operate over a very wide temperature (-273 to $>1000\ °C$) and pressure (UHV to $\gg 100$ atm) range, and (3) provide molecular level information about metal oxides makes Raman spectroscopy the most informative characterization technique for understanding the molecular structure and surface chemistry of the catalytic active sites present in metal oxide heterogeneous catalysts. The recent use of hyphenated Raman spectroscopy instrumentation (*e.g.*, Raman–IR, Raman–UV-vis, Raman–EPR) and the *operando* Raman spectroscopy methodology (*e.g.*, Raman–MS and Raman–GC) is allowing for the establishment of direct structure–activity/selectivity relationships that will have a significant impact on catalysis science in this decade. Consequently, this *critical review* will show the growth in the use of Raman spectroscopy in heterogeneous catalysis research, for metal oxides as well as metals, is poised to continue to exponentially grow in the coming years (173 references).

*Operando Molecular Spectroscopy & Catalysis Laboratory,
Department of Chemical Engineering, Bethlehem, PA 18015, USA.
E-mail: iew0@lehigh.edu; Fax: 1 610 758 5057; Tel: 1 610 758 4274*
† Part of the themed issue covering recent advances in the *in-situ* characterization of heterogeneous catalysts.

Introduction

Molecular vibrations give rise to both IR and Raman observable bands with each molecular structure providing its own set of vibrations.[1] The ability of Raman and IR

Israel E. Wachs

Israel E. Wachs studied chemical engineering at City College of the City University of New York and Stanford University. After several years at Exxon, he joined Lehigh University's Department of Chemical Engineering where he is the G. Whitney Snyder endowed professor and director of the Operando *Molecular Spectroscopy & Catalysis Laboratory. He received awards for his research on the determination of electronic and molecular structures of* catalytic active sites and their relationship to specific catalytic activity/selectivity (ACS Olah Award in Hydrocarbon or Petroleum Chemistry, Herman Pines Catalysis Award, AIChE Catalysis and Reaction Engineering Practice Award, EPA Clean Air Excellence Award).

Charles A. Roberts

Charles A. Roberts received his BS in Chemical Engineering from the University of Notre Dame. He is currently a PhD student in chemical engineering at Lehigh University under Professor Israel E. Wachs in the Operando Molecular Spectroscopy & Catalysis Research Laboratory. He has published on Raman and UV-vis spectroscopy of metal oxides. For his thesis, he is studying the structure–photoactivity relationships of model metal oxide photocata-*lysts with time-resolved* operando *Raman, UV-vis and FT-IR spectroscopy. He has participated in the NSF International Research and Education in Engineering program, studying in Caen, France under Prof. Marco Daturi; Lille, France under Prof. Edmond Payen; and Delft, The Netherlands under Prof. Guido Mul.*

spectroscopy to discriminate among multiple structures and functionalities uniquely endows them with molecular spectroscopic information, which is critical for discriminating among multiple catalytic active sites that may simultaneously be present. Whereas IR spectroscopy detects vibrations involving a change in dipole moment, Raman spectroscopy detects vibrations involving a change in polarizability. Neither spectroscopy, however, can detect ionic bonds. These complementary selection rules result in Raman spectroscopy generally being more sensitive to symmetric modes and IR spectroscopy typically being more sensitive to asymmetric modes. The high sensitivity of IR spectroscopy to changes in the dipole moment gives rise to strong signals from water and hydroxyls, but no signal from diatomic molecules (H_2, O_2, N_2, etc.) that do not have a dipole moment. In contrast, the low sensitivity of Raman spectroscopy to changes in dipole moment results in very weak signals from water and hydroxyls, but can detect diatomic molecules. An important consequence of these vibrational selection rules is that Raman spectroscopy can monitor vibrations in aqueous phases while IR spectroscopy is not able because of the strong absorption of the IR signal by the aqueous phase. In practice, IR spectroscopy usually gives rise to stronger signals of surface chemical probes (CO, CH_3OH, pyridine, etc.)[2] and surface hydroxyls (M–OH) while Raman spectroscopy results in stronger signals of inorganic catalytic active sites (e.g., M=O, M–O–M, M–O–M′ and M–O vibrations).[3] For many systems, IR spectroscopy may also be able to detect surface M=O functionalities which can be compared with the corresponding M=O Raman vibration for a more complete structural assignment based on vibrational selection rules.[4] Consequently, whereas IR spectroscopy is mostly employed to determine the chemical properties of the catalytic active sites (redox, basic and Lewis or Brønsted acid),[2] Raman spectroscopy is the vibrational spectroscopy of choice for directly determining the molecular structure of the catalytic active sites under all environmental conditions (aqueous as well as all temperatures and pressures).[5] For a more extensive discussion of the pros and cons of Raman and IR spectroscopy for characterization of catalytic active sites, the reader is referred to refs. 3–5. For detailed discussions of Raman theory,[1,3,4,5] instrumentation,[3,5] reaction cells[3,5] and experimental methodology,[3,5] the reader is referred to the indicated references.

The ability of Raman spectroscopy to provide detailed molecular structural information about the nature of the catalytic active sites, especially under various environmental conditions, has resulted in an explosion of Raman catalyst studies reported in the catalysis literature after 1995 as shown in Fig. 1. Publications during the early period of ~1970–1980 can be termed "exploratory" since these studies were primarily examining the kind of information that can be provided with Raman spectroscopy.[6–13] The ~1980–2000 period can be referred to as the "pioneering" period since these seminal studies began to employ controlled atmosphere or in situ conditions to determine the nature of the catalytic active sites present under catalytic reaction conditions.[13–37] The in situ Raman spectroscopy studies now account for about ~25% of all of the reported Raman publications and reflect the realization that the molecular structures of the catalytic

active sites dynamically respond to reactive environments (reactant concentration, T and P).[2–5] In the past few years, operando Raman spectroscopy studies have begun to appear that simultaneously combine direct in situ Raman spectroscopic observation of the catalysts and online reaction product analysis (conversion and selectivity) during relevant catalytic reaction conditions.[38] Only cutting edge operando Raman spectroscopy studies, to be covered below, will allow for directly establishing catalytic active site molecular structure–activity/selectivity relationships for catalytic systems and such studies are poised to significantly increase in the coming years and advance the foundation of catalysis science.

This contribution will demonstrate the type of direct, fundamental molecular structural information about catalytic active sites that can be obtained with Raman spectroscopy under all environments (aqueous, ambient, dehydrated and under reaction conditions). Special emphasis will be placed on mixed oxide catalysts because of their strong Raman signals. Advanced Raman techniques (UV Raman, SERS, TERS, etc.) and Raman microscopy will be covered by others in this special RSC issue.

Aqueous solutions

Raman spectroscopy is readily able to monitor metal oxide complexes in aqueous solutions that are employed to deposit catalytic active site precursors on high surface area oxide supports (e.g., Al_2O_3, TiO_2, ZrO_2, SiO_2, etc.) or to form mixed metal oxide catalysts that may be supported as well as unsupported. The Raman spectra of aqueous ammonium heptamolybdate, $(NH_4)_6Mo_7O_{24}\cdot4H_2O$, as a function of solution pH are presented in Fig. 2. The solution pH was adjusted by addition of acidic HCl or basic $NH_4\cdot H_2O$. At the highest pH value, Raman bands are present at 903 (v_s, symmetric stretch), 844 (v_{as}, asymmetric stretch) and 326 (δ, symmetric bending) cm^{-1}, with the band at ~173 cm^{-1} coming from the glass container holding the liquid, that are from the isolated $[MoO_4]^{2-}_{(aq)}$ anion. Lowering the aqueous solution pH to 6.16 introduces new Raman bands at 940 (v_s), 900 (v_{as}), 364 (δ) and new bands due to the presence of bridging Mo–O–Mo bonds (547 (v_{as}), 442 (v_s) and 218 (δ) cm^{-1}) that are related to $[Mo_7O_{24}]^{6-}_{(aq)}$ species. At the lowest solution pH of 2.95, Raman bands are present at 965 (v_s), 927 (v_{as}), 850 (v_{as}), 369 (δ) and bridging Mo–O–Mo vibrations at 534 (v_s) and 215 (δ) cm^{-1} from $[Mo_8O_{26}]^{4-}_{(aq)}$ anions. At the intermediate pH values of 7.00 both the $[MoO_4]^{2-}_{(aq)}$ and $[Mo_7O_{24}]^{6-}_{(aq)}$ anions coexist, while both $[Mo_7O_{24}]^{6-}_{(aq)}$ and $[Mo_8O_{26}]^{4-}_{(aq)}$ species are present at the pH value of 4.20. Only these three molybdate anions are present in aqueous solutions as a function of solution pH and molybdate concentration[39] and demonstrate the exquisite capability of Raman spectroscopy in discriminating among different molecular structures. The same three molybdate species have also been found to be present when an aqueous solution of ammonium heptamolybdate is impregnated into the pores of high surface area oxide supports.[40–43] Such catalysts are subsequently dried and calcined in an oxidizing environment at elevated temperatures to burn off the ammonium ligands and assure the complete oxidation of the supported molybdenum oxide phase.[40–43]
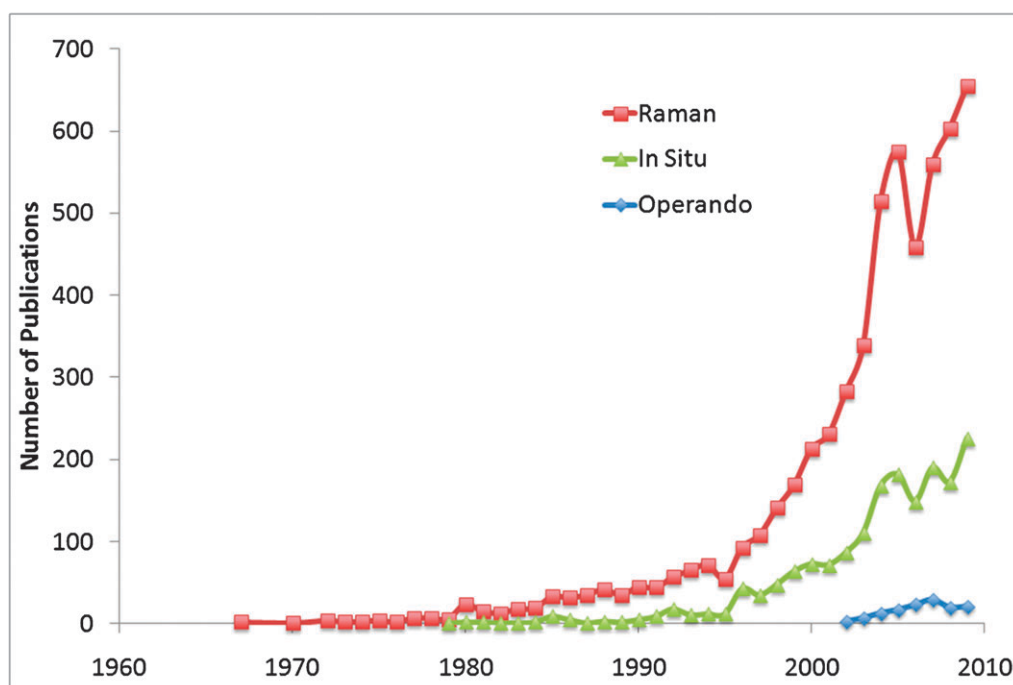
Fig. 1 Chronology of occurrences of Raman spectroscopy containing publications in heterogeneous catalysis literature.
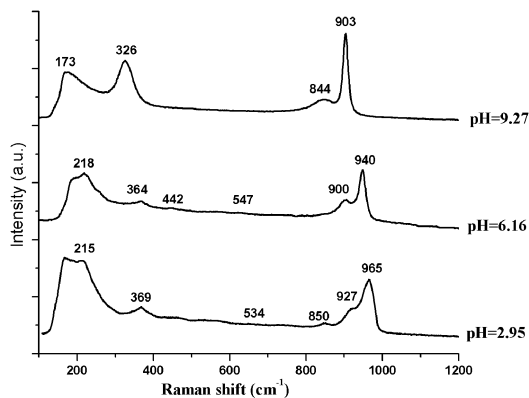

Fig. 2 Raman spectra of aqueous 0.2 M $(NH_4)_6Mo_7O_{24}$ solutions as a function of solution pH. Note, the 173 cm^{-1} band is from the glass dish used to hold the aqueous molybdena solution.

Vanadium peroxo–oxo complexes in aqueous solution possess both vanadyl V=O oxo and peroxo $V–O_2$ complexes.[44] It is not immediately clear which of the Raman bands at 967, 932 and 575 cm^{-1} for vanadium peroxo-oxo complexes are related to the V=O and $V–O_2$ vibrations, and discrimination between these two functionalities can be assisted with isotopic ^{18}O exchange studies since the molecular vibrations are mass dependent. Exposure to $H_2^{18}O$ selectively exchanges with the vanadyl V=O functionality (v_s(V=O) shifts from 967 → 929 cm^{-1}), but not the peroxo $V–O_2$ functionality. The facile ^{18}O exchange between $H_2^{18}O$ and the V=^{16}O functionality occurs *via* formation of the transient V–OH complex in the aqueous environment and the absence of $H^{18}O^{18}OH$ in the aqueous solution precludes exchange with the vanadium peroxo functionality. Exposure to $H^{18}O^{18}OH$, however, selectively exchanges with the peroxo $V–O_2$ functionality (v_s(O–O) shifts from 932 → 881 cm^{-1} and

v_s($V–O_2$) shifts from 575 to 547 cm^{-1}) and not the vanadyl functionality. Such selective isotopic tagging allows for clear assignments of the Raman bands originating from the peroxo $V–O_2$ functionality and the vanadyl V=O oxo functionality.

Supported metal oxide catalysts

Ambient conditions

For supported metal oxide catalysts, the metal oxide precursor solution is impregnated into the pores of the support and the impregnated catalyst is dried and, subsequently, calcined at elevated temperatures. The finished calcined catalysts are almost always exposed to ambient air by being saved in a bottle or transferred to a catalytic reactor. Under ambient conditions, the supported metal oxides have been found to contain ~20 layers of moisture that converts the molecular structure of the supported metal oxide phase to the same anionic species found in aqueous solutions.[45] The Raman spectra of supported molybdenum oxide catalysts on Al_2O_3 and SiO_2 under ambient conditions and after calcination are presented in Fig. 3(a) and (b), respectively. The Al_2O_3 support does not give rise to Raman active modes. The Raman spectrum of supported 1% MoO_3/Al_2O_3 under ambient conditions exhibits bands at 912, 846 and 312 cm^{-1} that are similar to the Raman bands characteristic of $[MoO_4]^{2-}_{(aq)}$ at 903, 844 and 326 cm^{-1}. The slight perturbations and broadening of the Raman bands for the alumina-supported $[MoO_4]^{2-}_{(aq)}$ species are a consequence of the interaction of the hydrated molybdate species with the alumina support surface. The Raman spectrum of supported 20% MoO_3/Al_2O_3 under ambient conditions gives rise to bands at 950, 846, 561, 367 and 215 cm^{-1} that are quite similar to that of $[Mo_7O_{24}]^{6-}_{(aq)}$ with Raman bands at 940, 900, 547, 442, 364 and 218 cm^{-1}. The pronounced shoulder at 846 cm^{-1} indicates that some
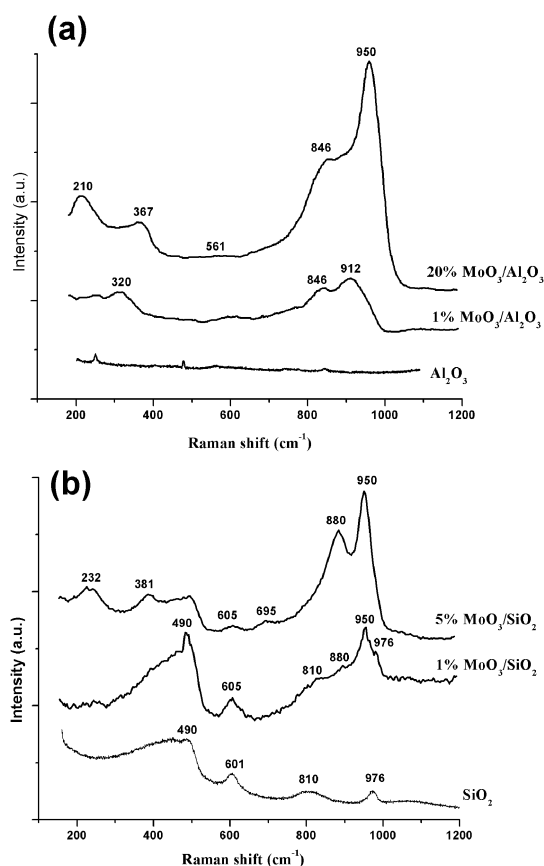
Fig. 3 Raman spectra of supported MoO_3/Al_2O_3 (a) and MoO_3/SiO_2 (b) catalysts under ambient conditions after calcination as a function of surface molybdena coverage.

$[MoO_4]^{2-}_{(aq)}$ species also coexist for the hydrated supported 20% MoO_3/Al_2O_3 catalyst. The corresponding Raman spectra of supported MoO_3/SiO_2 catalysts under ambient conditions are also depicted in Fig. 3b. The SiO_2 support possess several Raman active modes at 976 cm^{-1} (Si–OH), 810 (Si–O–Si), 601 (three-membered SiO rings), 490 (four-membered SiO rings) and 410–450 cm^{-1} (network bending). Unlike the supported 1% MoO_3/Al_2O_3 catalyst, the Raman spectrum of supported 1% MoO_3/SiO_2 under ambient conditions contains molybdate bands at 950 and 880 cm^{-1} that match those of $[Mo_7O_{24}]^{6-}_{(aq)}$ at 940 and 900 cm^{-1}. The strong Raman bands from the SiO_2 support at 976, 810, 605 and 490 cm^{-1} prevent detection of the additional molybdate bands in these regions. With higher molybdenum oxide concentrations, however, most of the Raman bands of the $[Mo_7O_{24}]^{6-}_{(aq)}$ species are observable for the supported 5% MoO_3/SiO_2 catalyst under ambient conditions at 950, 880, 381 and 232 cm^{-1}. The hydrated molybdate structures are dependent on pH of the thin aqueous layer present on these oxide catalysts, which is determined by the net pH at point of zero charge (PZC).[45] The PZC value for SiO_2 is ~ 3 and for Al_2O_3 ~ 9. This is why for the supported 1% MoO_3 catalysts $[MoO_4]^{2-}_{(aq)}$ is present on the Al_2O_3 support and $[Mo_7O_{24}]^{6-}_{(aq)}$ is present on the SiO_2 support at these low molybdenum oxide loadings. At high molybdenum oxide loading, the net pH at PZC is an average of the pH at PZC values of the oxide support and that of molybdenum oxide that has a pH at PZC of ~ 1. This is the reason that supported 20%

MoO_3/Al_2O_3 under ambient conditions primarily possesses $[Mo_7O_{24}]^{6-}_{(aq)}$ anions. Hydrated $[Mo_8O_{26}]^{4-}_{(aq)}$ species are rarely observed for supported molybdenum oxide catalysts under ambient conditions and can only be present at very high molybdenum oxide loading.[29,40] Thus, the same three hydrated molybdate anions are present in both aqueous solutions and on oxide supports under ambient conditions. Molecular structural information about the nature of the hydrated species present for many supported metal oxide catalyst systems under ambient conditions can be found in ref. 45.

A special outcome of the aqueous chemistry in the thin moisture layers is that the oxide support can under special pH conditions also dissolve in the aqueous film and subsequently react with the hydrated supported metal oxide phase to form a new complex. This is what takes place when supported MoO_3/SiO_2 catalysts are exposed to high moisture content at room temperature for an extended period of time.[19,28,46] The conversion of $[Mo_7O_{24}]^{6-}_{(aq)}$ anions (Raman bands at 950, 880, 695, 381 and 232 cm^{-1}) to silicomolybdic acid $[SiMo_{12}O_{40}]^{4-}_{(aq)}$ Keggin clusters (Raman bands at 978, 946, 614 and 241 cm^{-1}) under flowing H_2O/O_2 at room temperature is shown in Fig. 4. The silicomolybdic acid Keggin clusters only form at room-temperature conditions where the surface moisture content is greatest and thermally decompose as the surface moisture content is diminished upon heating to 300 °C. Thus, the silicomolybdic acid clusters can only be catalytic active sites for reactions conducted below 300 °C. Analogous behavior has been found for supported MoO_3/Al_2O_3 catalysts that form aluminomolybdic acid clusters.[47,48]

Dehydrated conditions

The surface moisture content on oxide surfaces is extremely small as temperatures of 300 °C are approached and the hydrated metal oxide complexes become dehydrated and decompose to spontaneously disperse and anchor to the oxide support surface hydroxyls.[19,28] The Raman spectra for dehydrated supported MoO_3/Al_2O_3 and MoO_3/SiO_2 catalysts are presented in Fig. 5(a) and (b), respectively, and are very different than their spectra under ambient conditions reflecting their molecular structural transformations upon dehydration
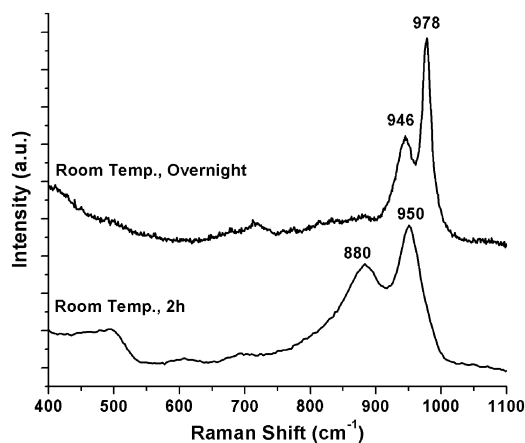
Fig. 4 *In situ* Raman spectra of 5% MoO_3/SiO_2 in flowing air saturated with water at room temperature for 2 h and room temperature overnight.
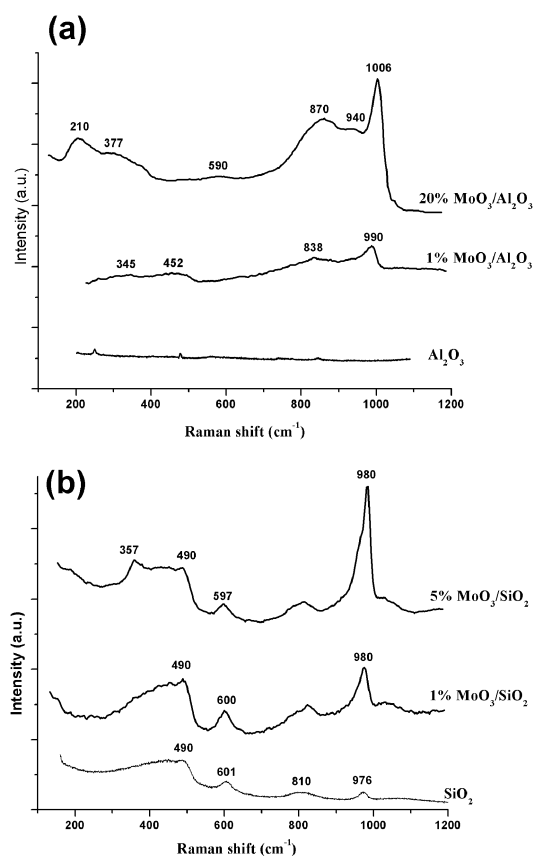
**Fig. 5** *In situ* Raman spectra of supported MoO_3/Al_2O_3 (a) and MoO_3/SiO_2 (b) catalysts under dehydrated conditions as a function of surface molybdena coverage.

(compare Fig. 3 and 5). The Raman spectra of the dehydrated supported MoO_3/SiO_2 catalysts give rise to new Raman bands at 980 (v_s), 965 (v_{as}) and 357 (δ) cm^{-1} that have been assigned to isolated surface dioxo $(O\!\!=\!\!)_2Mo(-O-Si)_2$ species.[49–53] The dehydrated supported 1% MoO_3/Al_2O_3 catalyst exhibits Raman bands at 990 (v_s), 838 cm^{-1} (v_s Mo–O–Al), 452 (v_s Mo–O–Mo) and 345 (δ) that have been assigned to isolated surface $(O\!\!=\!\!)_2Mo(O-Al)_2$ species.[53] At high molybdenum oxide loading that approaches monolayer coverage, the Raman spectrum of the dehydrated supported 20% MoO_3/Al_2O_3 catalyst possesses bands at 1006 (v_s), ~940 (v_{as}), ~870 (v_s Mo–O–Al), ~560 (v_s Mo–O–Mo), 377 (δ) cm^{-1} and 210 (δ Mo–O–Mo) cm^{-1}. The shift of the v_s Mo=O mode from ~990 to 1006 cm^{-1} and the presence of bridging Mo–O–Mo vibrations reveals the transformation of the dehydrated isolated surface dioxo $(O\!\!=\!\!)_2MoO_2$ species to dehydrated polymeric surface mono-oxo O=MoO_4 species with surface molybdenum oxide coverage on Al_2O_3.[53] Some dehydrated, isolated surface dioxo $(O\!\!=\!\!)_2MoO_2$ species also coexist with the dehydrated, polymeric surface mono-oxo O=MoO_5 units at monolayer coverage on Al_2O_3 and can be more easily detected by UV-vis. The intensity of the Raman bands from the surface polymers, however, are stronger than the Raman bands of the surface monomers due to their shorter Mo=O bonds that result in greater Mo=O electron density (leading to greater change in electron polarizability). Thus, the molecular structures of the catalytic active sites of dehydrated

surface metal oxide species on oxide supports tend to be isolated at low surface coverage and can have coexisting isolated and polymeric species at high surface coverage. The Raman spectra and molecular structures of the dehydrated supported V_2O_5,[49,54–64] Nb_2O_5,[49,65,66] Ta_2O_5,[49,67–69] CrO_3,[49,70–74] MoO_3,[49,75,76] WO_3,[77–82] and Re_2O_7[49,83] catalyst systems have been reported in recent years. Although there is still some discussion in the literature about the assignments of some of the vibrational bands, the Raman spectra are completely reproducible from lab to lab.

Additional fundamental insight into the origin of specific vibrations and molecular structures of the supported metal oxide catalytic active sites can be obtained from isotopic exchange studies since the Raman vibrations are quite sensitive to the mass of the vibrating atoms.[1] For example, substitution of ^{16}O by ^{18}O or H by D can dramatically shift the Raman bands to lower wavenumbers because of the greater mass of the isotopes, by as much as 10–700 cm^{-1}, which is readily detectable. Substitution of ^{18}O for ^{16}O, usually performed by exposure to either gaseous $^{18}O_2$ or $H_2^{18}O$, reveals which of the Raman bands in a spectrum originate from oxygen-containing functionalities. For dehydrated supported 8% MoO_3/SiO_2, oxygen exchange shifts the dioxo surface MoO_4 bands from 988 (v_s)/970 (v_{as}) to 938 (v_s)/ 920 (v_{as}) cm^{-1} and the mono-oxo surface MoO_5 bands from 1020 (v_s) to 998 (v_s) cm^{-1} as shown in Fig. 6. In addition, the MoO_x bending mode shifts from 364 to 352 cm^{-1}. The shift of these bands confirms that they are indeed related to Mo–O vibrations and the manner in which they shift during time-resolved oxygen exchange also provides for discrimination between mono-oxo and dioxo structures. For mono-oxo molybdate structures, the Mo=^{16}O band continuously decreases in intensity and does not alter its position as the intensity of the Mo=^{18}O band continuously increases. For dioxo molybdate structures, the Mo=^{16}O band intensity, initially at 988 cm^{-1}, both decreases in intensity and also shifts position to lower wavenumber, 978 cm^{-1} at 50/50 oxygen exchange, as the intensity of the Mo=^{18}O bands increases. The Raman shift of 988 to 978 cm^{-1} with oxygen exchange results from the presence of $^{18}O\!\!=\!\!Mo\!\!=\!\!^{16}O$ species
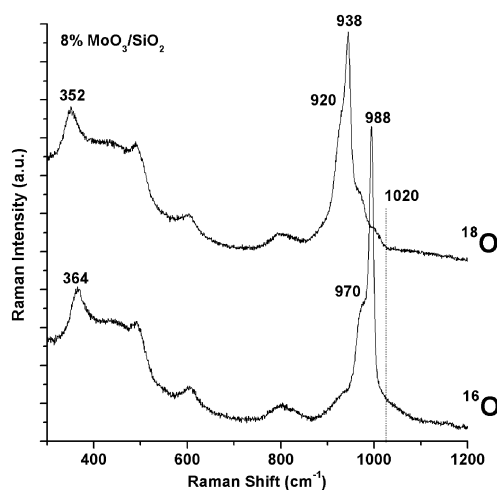
Fig. 6 *In situ* Raman spectra (325 nm excitation) of dehydrated supported 8% MoO_3/SiO_2 at 450 °C: ~100% ^{16}O and ~100% ^{18}O.

at intermediate extents of oxygen exchange. Note that the major Si–O vibrations of the SiO$_2$ support are not perturbed by the isotopic ^{18}O exchange in the surface MoO$_x$ species reflecting the lack of redox characteristics of silica. Additional insight into the presence of –OH functionalities in supported MoO$_3$/SiO$_3$ catalysts was obtained by isotopically exchanging the –OH to –OD functionalities by exposure to D$_2$O. First, the exchange with D$_2$O does not perturb any of the bands from the surface MoO$_4$ and MoO$_5$ species on SiO$_2$ indicating that there is no Mo–OH functionality in these surface molybdenum oxide species on silica. The absence of a M–OH functionality for other silica-supported metal oxide systems (VO$_x$, NbO$_x$, TaO$_x$, CrO$_x$, WO$_x$ and ReO$_x$) was also confirmed with similar H–D exchange studies.[49] Second, the Raman bands due to the Si–OH functionality are perturbed with the Si–(OH) vibration at 970 cm^{-1} shifting to $\sim$950 cm^{-1} for Si–(OD) and the SiO–(H) vibration at 3740 cm^{-1} shifting to 2770 cm^{-1} for SiO–(D).[49] In summary, isotopic exchange studies are extremely informative, as already shown above for the aqueous vanadium peroxo–oxo complex, about the origin of different vibrational bands that provide detailed molecular structural information about supported metal oxide catalytic active sites.

Reaction conditions (temperature, pressure and phase)

Thermal treatments at elevated temperatures and exposure to reactive environments may also alter the molecular structures of the surface metal oxide catalytic active sites and, thus, it is critical to perform Raman spectroscopic characterization under relevant reaction conditions and temperatures to determine the actual structures of the catalytic active sites that are present.

Thermal treatments in O$_2$ environments

The effect of raising the catalyst temperature on the molecular structure of dehydrated supported WO$_3$/SiO$_2$ in flowing oxygen is shown in Fig. 7. At lower temperatures, Raman bands are present at 985 and 1010 cm^{-1} that originate from isolated surface dioxo (O=)$_2$W(O–Si)$_2$ and isolated surface mono-oxo O=W(O–Si)$_4$ species. As the catalyst temperature is increased, the isolated surface dioxo WO$_4$ catalytic active sites are converted to the isolated surface mono-oxo O=W(O–Si)$_4$ catalytic active sites. However, for most supported metal oxide catalytic active sites, their molecular structures remain the same as a function of temperature within a mild temperature regime.[3,5] At extremely high temperatures ($T > 600\,^\circ$C), however, the BET surface area of catalysts will begin to dramatically decrease and will have a significant effect upon the molecular structures of the supported metal oxide phase. For example, heating supported WO$_3$/Al$_2$O$_3$ catalysts to 800–1100 $^\circ$C collapses the Al$_2$O$_3$ surface area below that required to maintain a dispersed surface tungsten oxide monolayer.[84] Such a situation does not allow maintaining the entire supported tungsten oxide phase as a two-dimensional phase and the tungsten oxide in excess of monolayer coverage can not be accommodated in the monolayer phase. Consequently, a portion of the surface tungsten oxide species is initially converted to crystalline WO$_3$ nanoparticles (NPs). As the temperature is further increased, the WO$_3$ NPs react with alumina from the Al$_2$O$_3$
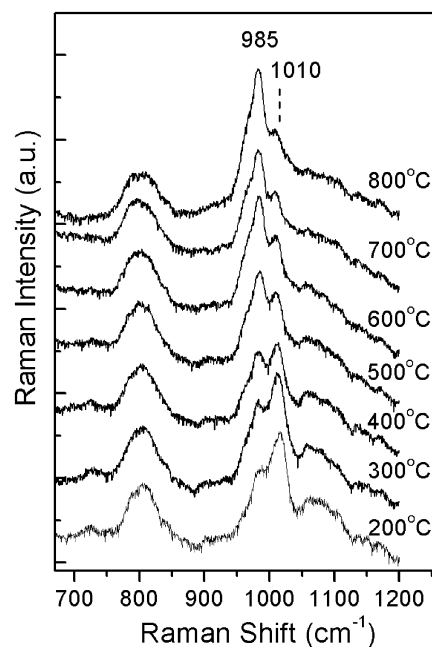

Fig. 7 *In situ* Raman spectra showing the temperature dependence of the molecular structure of dehydrated supported WO$_3$/SiO$_2$ in flowing oxygen.

support to form crystalline Al$_2$(WO$_4$)$_3$ NPs, which represent the most thermodynamically stable state for the WO$_3$–Al$_2$O$_3$ system. The above examples demonstrate that it is always necessary to ascertain that the molecular structures of the catalytic active sites are not altered by the temperature of calcination and the catalytic reaction.

Solid catalysts produce strong radiation emission in the visible region (>400 nm) at temperatures above $\sim$750 $^\circ$C that usually prevents collection of visible Raman spectra at such elevated temperatures. UV Raman spectroscopy, with excitation below 400 nm is not affected by this strong radiation emission, and allows collection of Raman spectra at such extreme temperatures. A comparison of the visible and UV Raman spectra for a supported Pd/Al$_2$O$_3$ catalyst at 800 $^\circ$C in an O$_2$/He environment is presented in Fig. 8. The visible Raman spectrum of the oxidized supported Pd/Al$_2$O$_3$ catalyst contains a strong emission background, especially above $\sim$1200 cm^{-1}, that completely overwhelms the vibrations from the oxidized supported Pd/Al$_2$O$_3$ catalyst. The Raman bands at $\sim$600 (Pd–O vibration) and $\sim$1200 (first overtone of Pd–O vibration) cm^{-1} are from the alumina-supported PdO$_x$ component and the bands at $\sim$430 and $\sim$790 cm^{-1} are from the quartz window of the environmental cell. With the ability of UV Raman spectroscopy to collect radiation emission-free spectra at extreme temperatures, the only limitation becomes the temperature limits of the *in situ* environmental cell and the lenses used to collect the scattered Raman light (see section below on reaction environments for an even higher temperature example).

Thermal treatments in H$_2$ environments

The supported metal oxide catalysts usually become partially or fully reduced by exposure to H$_2$ at elevated temperatures.
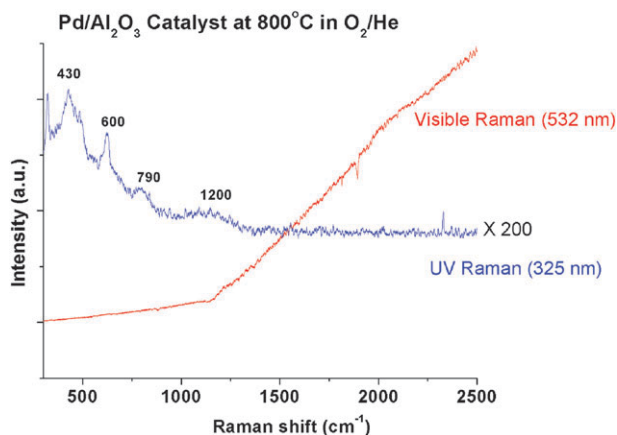
Fig. 8 Comparison of visible (532 nm) and UV (325 nm) Raman spectra for a supported Pd/Al$_2$O$_3$ catalyst at 800 °C in an O$_2$/He environment.

Such reducing treatments can further identify the Raman bands originating from the supported metal oxide phase and sometimes can also discriminate between the bands from different surface metal oxide species in the case of the simultaneous presence of several surface species. For example, exposing supported Re$_2$O$_7$/SiO$_2$ catalysts to H$_2$ reduction completely reduces the surface ReO$_4$ catalytic active site (1010 (v_s), 977 (v_{as}) and 343 (δ) cm^{-1}) and only the vibrations of the SiO$_2$ support remain (3740, 970, 800, 605, 487–450 cm^{-1}).[49] For the supported CrO$_3$/SiO$_2$ catalyst system, the Raman spectra possess two strong bands that may be from either the v_s/v_{as} vibrations of a surface dioxo (O=)$_2$CrO$_2$ unit or from two different surface CrO$_x$ species at 1011 and 982 cm^{-1}.[49] Time-resolved reduction of the supported CrO$_3$/SiO$_2$ catalyst with H$_2$/He at 500 °C reveals that the 982 cm^{-1} band preferentially reduces over the 1011 cm^{-1} band.[49] This important observation demonstrates that the two Raman bands are from two different surface CrO$_x$ species: the band at 982 cm^{-1} is the v_s vibration of the surface dioxo species and the band at 1011 cm^{-1} is the v_s of a mono-oxo surface CrO$_x$ species. This reduction study also reveals that the dioxo surface CrO$_4$ species is more reactive towards reduction than the mono-oxo surface CrO$_x$ species, which is an important molecular structure–reactivity relationship.

Chemisorbed molecular O$_2$ species

The thermal treatments in H$_2$ environments produce reduced metal oxide sites that are oxygen deficient (contain atomic oxygen vacancies). Low-temperature chemisorption of gaseous molecular O$_2$ on such defective metal oxide surfaces can yield surface superoxide O$_2^-$ and peroxide O$_2^{2-}$ species. For example, chemisorption of molecular ^{18}O$_2$ on pre-reduced supported 3% V$_2$O$_5$/CeO$_2$ catalyst at −180 °C, which contains monolayer surface coverage of VO$_x$ species, forms new Raman bands at 1096 (v_s of V–^{18}O–^{18}O$^-$ surface superoxo), 830 (v_s of V–^{18}O$_2$ or V–^{18}O–^{18}O–V surface peroxo) and 530 cm^{-1} (v_s of surface V–^{18}O$_2$ peroxo) with the intensity of the Raman band from the surface superoxo being much stronger than that of the surface peroxo. The surface V-superoxo and V-peroxo species are thermally stable up to −60 °C at which point they decompose and reform the vanadyl

V=O bond. The low thermal stability of the surface V–O–O$^-$ superoxo and V–O$_2^-$ peroxo species reveals that such surface intermediates have extremely short lifetimes at 200–600 °C and will not be stable or detectable under typical oxidation reaction conditions. Nevertheless, surface superoxo and peroxo species are routinely invoked in mechanisms of selective oxidation reactions in the heterogeneous catalysis literature. These new findings suggest that surface M–O–O$^-$ superoxo and M–O$_2^-$ or M–O–O–M peroxo reaction intermediates are too short lived to form stable surface intermediate complexes with gaseous reactants at elevated reaction temperatures.

Reaction environments: gas phase

During methanol oxidation at the mild reaction temperature of 230 °C, the isolated surface WO$_x$ species on SiO$_2$ are stable and represent the catalytic active sites.[30] Unlike the thermal stability of the surface WO$_4$ species on SiO$_2$ in O$_2$, both isolated surface dioxo MoO$_4$ and mono-oxo MoO$_5$ species are thermally stable on SiO$_2$ catalysts at elevated temperatures.[49] The surface MoO$_x$ species on SiO$_2$ are also stable during CH$_4$ oxidation to HCHO over supported MoO$_3$/SiO$_2$ catalysts at 550 °C.[27] The surface MoO$_x$ species on SiO$_2$, however, are unstable during methanol oxidation at 230 °C and transform to crystalline beta-MoO$_3$ NPs.[28] The structural change of the catalytic active site is driven by the formation of labile Mo–OCH$_3$ complexes that agglomerate the surface molybdenum oxide species under reaction conditions. The conversion of the surface MoO$_x$ species to crystalline beta-MoO$_3$ NPs is reflected in the lower catalytic activity and formaldehyde selectivity of the supported MoO$_3$/SiO$_2$ catalyst relative to other supported molybdenum oxide catalysts.[28]

There is currently much interest in autothermally reforming hydrocarbons at elevated temperatures to produce synthesis gas (H$_2$ and CO), which requires extreme reaction temperatures. The *in situ* UV Raman spectra of a supported Rh/Al$_2$O$_3$ catalyst under oxidizing conditions and during autothermal reforming of propane, with a C/O ratio of 1, at 1000 °C are presented in Fig. 9. Under oxidizing environments, the UV Raman spectra exhibit a broad band from the quartz window and the supported RhO$_x$ component between ∼450–800 cm^{-1}. During autothermal reforming of propane, the propane reduces the alumina supported RhO$_x$ phase and its Raman band at ∼600 cm^{-1} is absent with only the quartz window vibrations at ∼450 and ∼800 cm^{-1} remaining. In addition, new Raman bands appear at 1387 and 1585 cm^{-1} from deposited coke that is responsible for catalyst deactivation at these extreme reaction conditions. Switching back to oxidizing conditions, returns the catalyst to its initial oxidized state by burning off the deposited coke and oxidizing the reduced Rh phase to RhO$_x$.

These examples demonstrate the dynamic nature of the surface MoO$_x$-intermediate complexes that necessitate spectroscopic monitoring of the actual catalytic active sites under relevant reaction conditions.

Time-resolved *operando* molecular spectroscopy

For selective oxidation reactions over bulk and supported metal oxides, there is always a question of the source of the

5008 | *Chem. Soc. Rev.*, 2010, **39**, 5002–5017

This journal is © The Royal Society of Chemistry 2010
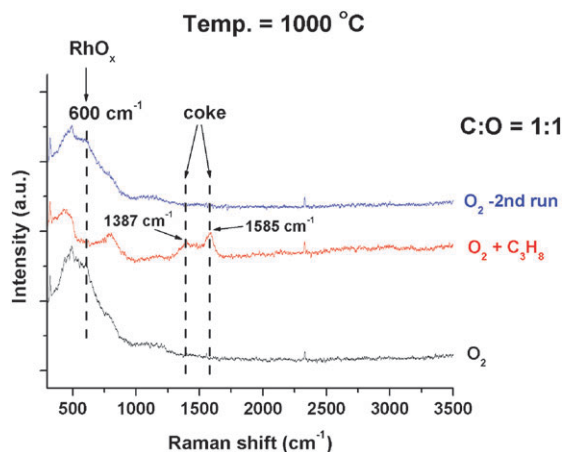
Fig. 9 *In situ* UV Raman spectra of supported RhO_x/Al_2O_3 under oxidizing and autothermal reforming of propane conditions: 1000 °C and $C:O = 1:1$.

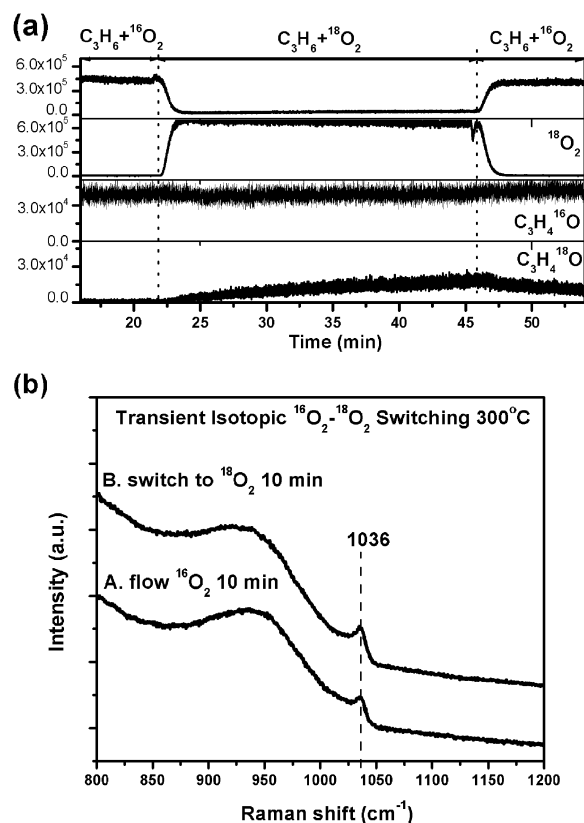**Fig. 10** *Operando* mass spectrometry (a) and Raman (b) spectra during transient isotopic $^{18}O_2$–$^{16}O_2$ switching experiment for steady-state propylene oxidation to acrolein at 300 °C over a supported V_2O_5/Nb_2O_5 monolayer catalyst.

oxygen that is involved in the rate-determining-step (rds) of the oxidation reaction. For example, the oxygen may be present as dissociated surface O_{ads} that is in equilibrium with gaseous molecular O_2 (Langmuir–Hinshelwood mechanism) or the oxygen may be supplied by the catalyst lattice (Mars–van Krevelen mechanism).[85] To distinguish between these two mechanistic scenarios, it is necessary to switch oxygen isotopes and simultaneously monitor in real-time the evolution of the oxygen in the catalyst lattice and in the reaction products (an *operando* spectroscopy study). For propylene oxidation to acrolein ($H_2C=CHCHO$) over a supported V_2O_5/Nb_2O_5 catalyst containing a monolayer surface VO_4 species, such a steady-state isotopic transient kinetic analysis (SSITKA) was performed as shown in Fig. 10a.[86] Switching gas-phase molecular $^{16}O_2$ to $^{18}O_2$ does not perturb the production of $H_2C=CHCH^{16}O$ that continues in the presence of gaseous molecular $^{18}O_2$. The absence of an immediate jump in the mass spectrometer signal for the production of the isotopically labeled $H_2C=CHCH^{18}O$ confirms that the oxygen involved in the rds of acrolein formation is coming from the catalyst lattice that contains O-16 rather than the molecular $^{18}O_2$ in the gas phase. Raman examination of the oxygen present in the surface VO_4 catalytic active sites on the Nb_2O_5 support directly confirms that the surface VO_4 catalytic active sites during propylene oxidation retain the O-16 isotope and do not possess the O-18 isotope as shown in Fig. 10b (the $V=^{16}O$ band occurs at 1036 cm^{-1} and the $V=^{18}O$ band would be expected at ~990 cm^{-1}).[87,88] The Mars–van Krevelen mechanism occurs because there is a rapid exchange between surface $^{18}O_{ads}$ and catalyst lattice ^{16}O from the Nb_2O_5 support, which must take place *via* the bridging V–O–Nb bond. Furthermore, the surface VO_4 sites remain fully oxidized during propylene oxidation ($C_3^= : O_2 = 1:4$) as revealed in Fig. 10b, and neither surface superoxide $V-^{18}O-^{18}O$ (expected at 1096 and 530 cm^{-1}) or peroxide $V-^{18}O_2$ (expected at 830 and 530 cm^{-1}) Raman bands are present during this oxidation reaction at 300 °C. As can be appreciated from this Raman–MS experiment, *operando* molecular spectroscopy studies are extremely informative about the molecular structure and oxidation state of the

surface metal oxide catalytic active sites during reactions and, in this case, reveal the specific oxidation mechanism (Mars–van Krevelen *vs.* Langmuir–Hinshelwood) that is taking place during selective oxidation of propylene to acrolein over the supported V_2O_5/Nb_2O_5 catalyst.

Bulk metal oxide catalysts

Pure metal oxides (one component)

In the absence of an oxide support, pure metal oxides will crystallize when calcined at elevated temperatures in an oxygen containing environment.[89] Such crystalline metal oxide phases are well-ordered and usually give rise to sharp Raman bands reflecting the local structure of the cations. If there is only one cation site in the crystal structure, then only one set of Raman bands will be observed. If the crystal structure contains multiple cation sites, then each cation will yield its own set of Raman bands.[1] The Raman bands of bulk crystalline phases generally become broader as their temperatures are increased (thermal broadening). The Raman bands of the bulk crystalline phases in bulk metal oxides are not sensitive to moisture since moisture cannot enter the bulk lattice.[89] The surfaces of bulk metal oxides, however, terminate in M=O and M–OH functionalities that are sensitive to the presence of moisture.[2–5] For example, comparison of the Raman spectra of bulk $Nb_2O_5 \cdot nH_2O$ under hydrated and dehydrated conditions
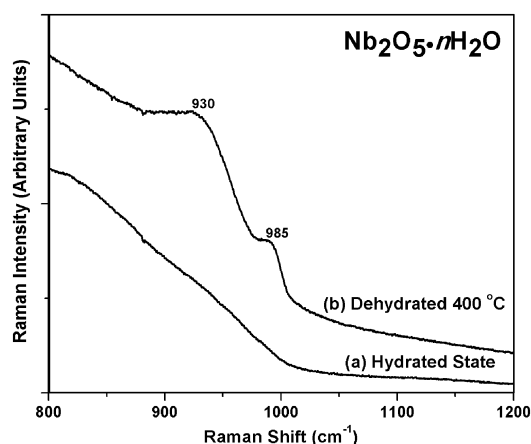
Fig. 11 *In situ* Raman spectra of $Nb_2O_5 \cdot nH_2O$: (a) hydrated state and (b) dehydrated at 400 °C and cooled to 50 °C under flowing oxygen.

in Fig. 11 reveals that surface $Nb{=}O$ moieties (~ 980 cm^{-1}) and surface $Nb{-}O{-}Nb$ moieties (~ 930 cm^{-1}) are present on the surface of bulk $Nb_2O_5 \cdot nH_2O$ since the $Nb{=}O$ and $Nb{-}O{-}Nb$ bonds are moisture sensitive.[90] Surface $M{=}O$ functionalities are generally present on the surfaces of group 5–7 metal oxides because of their high oxidation states. These surface $M{=}O$ moieties, as well as surface $M{-}O{-}M$ and $M{-}OH$ functionalities, represent the catalytic active sites of bulk metal oxides since this is where the reactants chemisorb on bulk metal oxide catalysts.

Bulk mixed metal oxides (two component)

Bulk mixed metal oxides are formed when two or more metal oxides, initially in the form of a metal oxide precursor or even as a pure metal oxide, are reacted by calcination in an oxidizing environment at elevated temperatures. The resulting bulk mixed metal oxides usually form well-ordered crystalline phases[89] that tend to usually exhibit sharp Raman bands.[3,5] Although the components are well mixed in the bulk phase, the component with the lowest surface free energy tends to surface segregate in bulk mixed metal oxides.[91] The Raman spectra of a series of co-precipitated V_2O_5–Nb_2O_5 bulk mixed oxides are presented in Fig. 12.[92] For 5% V_2O_5–Nb_2O_5, the Raman spectrum possesses bands at 980, 690, 640 and ~ 250 cm^{-1}. The 980 cm^{-1} band arises from vanadyl $V{=}O$ bonds of distorted VO_6 sites in the bulk of the $Nb_{2-x}V_xO_5$ mixed oxide. Further increasing the vanadium oxide content of $Nb_{2-x}V_xO_5$ introduces a new Raman band at 1020 cm^{-1} associated with the terminal vanadyl $V{=}O$ bonds of mono-oxo surface VO_4 species on the mixed oxide. At the highest vanadium oxide content of the $Nb_{2-x}V_xO_5$ mixed oxide, additional bands appear at 994, 697, 518, 404, 303, 284 and 144 cm^{-1} from crystalline V_2O_5 nanoparticles. Corresponding catalytic studies for propane oxidative dehydrogenation (ODH) revealed that the catalytic active sites for the $Nb_{2-x}V_xO_5$ mixed oxides are the surface mono-oxo VO_4 sites and not the VO_6 sites dissolved in the mixed oxide bulk that are not accessible to the propane reactant. Extensive detailed studies of bulk mixed metal molybdates under oxidizing and propane oxidation reaction conditions have been reported by Mestl.[93–95]
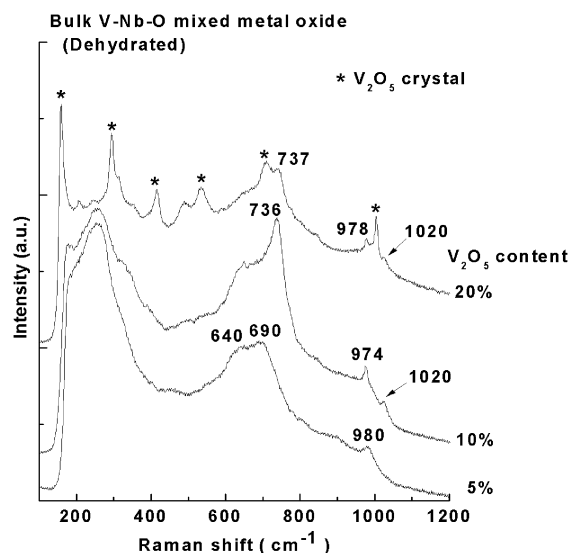
Fig. 12 *In situ* Raman spectra of bulk V_2O_5–Nb_2O_5 mixed metal oxides under dehydrated conditions.

Polyoxo metallates (POMs)

V-containing POMs are usually prepared by substituting redox VO_x units for acidic WO_x or MoO_x sites in the $H_3PW_{12}O_{40}$ and $H_3PMo_{12}O_{40}$ sub-nanometre Keggin structures, respectively.[42] The substituted VO_x units adopt distorted mono-oxo $O{=}VO_5$ coordination with four of the oxygen atoms bonded to adjacent W or Mo cations and the remaining oxygen atom weakly bonded to the central P heteroatom.[96–98] Typically, only 1–3 VO_x units are introduced into the Keggin structures since additional units can destabilize the POM.[99] It is generally assumed that all the VO_6 units have been substituted into the primary Keggin structure, but recent *in situ* Raman studies during methanol oxidation revealed that surface VO_x species can also be present on the outer surface of POMs secondary structure.[100] The Raman spectra of $H_3PW_{12}O_{40}$ (TPA), $H_4PW_{11}V_1O_{40}$ (TPAV1), $H_5PW_{10}V_2O_{40}$ (TPAV2), $H_6PW_9V_3O_{40}$ (TPAV3) and supported $VO_x/H_3PW_{12}O_{40}$ (VOTPA) during methanol oxidation by the VO_x redox sites and methanol dehydration by the WO_x acid sites are compared in Fig. 13. The V-free TPA Keggin retains its high degree of order under the reaction conditions as reflected by the sharp $W{=}O$ Raman band at 1022 cm^{-1}. The TPAV1, in which one VO_x unit has been substituted for WO_x in TPA, also gives rise to a relatively sharp $W{=}O$ Raman band at 1022 cm^{-1} that is slightly broadened by the insertion of the VO_x unit into the TPA Keggin structure under reaction conditions. Significant broadening of the $W{=}O$ 1022 cm^{-1} Raman band occurs for TPAV2 when two VO_x units are attempted to be introduced into TPA, which reflects structural disorder of the Keggin structure during methanol oxidation/dehydration. Attempts to introduce three VO_x units per Keggin structure (TPAV3) results in splitting of the $W{=}O$ band to form a second band at ~ 970 cm^{-1} in addition to the 1022 cm^{-1} band during methanol oxidation/dehydration. To better understand the origin of the $W{=}O$ band splitting, VO_x was also deposited on the outer surface of the TPA Keggin structure (VOTPA) and examined during methanol oxidation/dehydration.
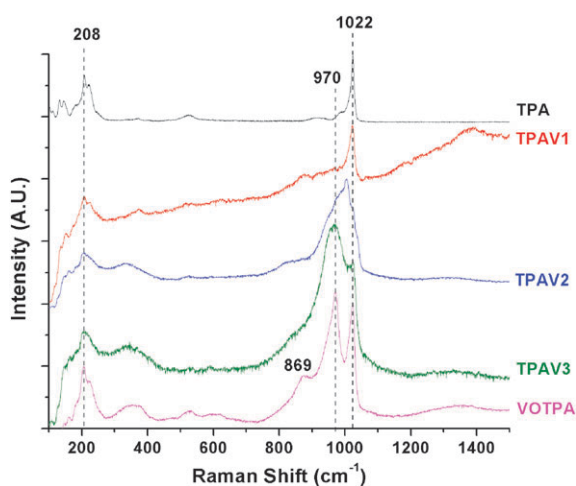
Fig. 13 *In situ* Raman spectra of TPA, TPAV and VOTPA Keggins during methanol oxidation/dehydration (O_2/CH_3OH = 2.17) at 250 °C).

The Raman spectrum of the VOTPA Keggin structure reveals that when VO_x units are present on the outer surface of TPA the W=O band splits into two bands at 970 and 1022 due to loss of vibrational coupling between adjacent W=O units in the Keggin structure. Furthermore, it is noted that the Raman bands for the VOTPA Keggin structure are sharp and not broadened as found for the TPAV Keggins, which reflects the disorder of the TPA Keggin structure caused by substitution of VO_x units for WO_x units in its primary structure. These structural changes and locations of the catalytic active VO_x redox sites have a profound effect on the methanol oxidation catalytic activity since the VO_x sites substituted into the primary Keggin structure are $100\times$ more active than the VO_x sites on the secondary Keggin structure or outer surface. Thus, the location of VO_x catalytic active sites in Keggins can be discriminated with *in situ* Raman spectroscopy and their location also affects the extent of disorder of the Keggin structure during catalytic reactions as well as their specific catalytic performance.

Layered metal hydroxides

Metal oxides, and especially vanadium oxide, have been successfully intercalated into layered metal hydroxides found in clays and hydrotalcites. Vanadium oxide was ion exchanged into the $Li_2Al(OH)_6^+$ layered hydroxide over the pH range of 3–11.[101] Characterization studies showed that the vanadia in the interlayer was present as hydrated $V_2O_7^{4-}$ and $V_4O_{12}^{4-}$ species at ambient conditions. Heating to ~ 100 °C induced transformation of $V_2O_7^{4-}$ to $V_4O_{12}^{4-}$ species in the interlayer, with further extent of polymerization upon heating to 350 °C. At higher temperatures the degradation of the layered framework took place with concomitant formation of crystalline Li_3VO_4 and $LiVO_3$. The hydrated vanadate species observed in these layered hydroxides are similar to those found on hydrated oxide surfaces of simple oxides and their structures only depend on the net pH at point of zero charge (PZC) of the hydrated interlayer [see above section on hydrated supported metal oxides]. Although no catalytic data have been reported for the intercalated vanadium oxides in clays, the catalytic properties of V-intercalated clays and
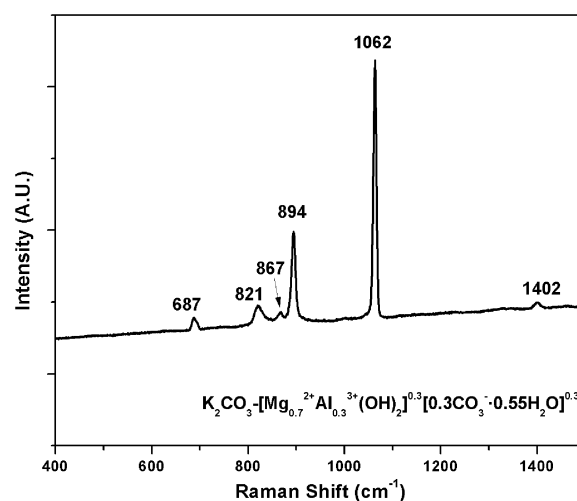
Fig. 14 *In situ* Raman spectrum of potassium carbonate treated hydrotalcite dehydrated under oxidizing conditions at 400 °C and the spectrum was collected at room temperature.

hydrotalcites should be related to those reported above for supported V_2O_5/Al_2O_3 and V_2O_5/MgO catalysts. The major difference between the vanadate species intercalated into the hydroxide layers and more traditional supported metal oxides is that the former tend to thermally decompose at rather mild temperatures (~ 350 °C) in the presence of vanadium oxide, which limits the use of clays and hydrotalcites as substrates for vanadium oxide at elevated temperatures. Raman spectra of layered metal hydroxides are still rather rare in the literature.

The potassium carbonate treated hydrotalcite $K_2CO_3 \cdot [Mg_{0.7}^{2+}Al_{0.3}^{3+}(OH)_2^{1-}]^{0.3}[0.3CO_3^{1-} \cdot 0.55H_2O]^{0.3}$ is employed for high temperature, reversible CO_2 capture from industrial waste streams.[102] The dehydrated *in situ* Raman spectrum of the potassium carbonate treated hydrotalcite is presented in Fig. 14. The Raman bands at 687 cm^{-1} [v_1(symmetric stretch)], 821, 867 and 894 cm^{-1} [v_2(asymmetric stretches)], 1063 cm^{-1} [v_3(asymmetric stretch)] and 1402 cm^{-1} [v_4(in-plane bending)] are from interlayer carbonates.[103] Crystalline K_2CO_3 nanoparticles also give rise to a strong Raman band at 1067 cm^{-1} that is slightly shifted from the hydrotalcite interlayer Raman band at 1063 cm^{-1}. It may be possible that a trace of crystalline K_2CO_3 is present in the potassium carbonate treated hydrotalcite given the close proximity of the two bands. The $[Mg_{0.7}^{+2}Al_{0.3}^{3+}(OH)_2^{1-}]$ component does not yield Raman active bands or give rise to very weak Raman signals that are significantly less intense than the interlayer carbonates. Thus, the $K_2CO_3 \cdot [Mg_{0.7}^{+2}Al_{0.3}^{3+}(OH)_2^{1-}]^{0.3}[0.3CO_3^{1-} \cdot 0.55H_2O]^{0.3}$ hydrotalcite stores the CO_2 as surface carbonate species in its hydroxide interlayers.

Zeolites

Zeolites are crystalline porous metal oxides possessing enormous internal surface area (1000 $m^2\ g^{-1}$), where every metal cation is either an internal or external surface site. Zeolites are composed of an aluminosilicate framework of the type $M_{x/n}[(AlO_2)_x(SiO_2)_y] \cdot yH_2O$ (in which n is the charge on the metal cation, M^{n+}, that typically is an alkali-metal ion). To form the acid form, the basic alkali-metal sites are

exchanged with protons to form the $H_{x/n}[(AlO_2)_x(SiO_2)_y] \cdot yH_2O]$. In contrast to the relatively few reported Raman spectra of layered hydroxides in the literature, Raman spectra of zeolites are now becoming more common in the literature and several reviews have appeared.[104–106] The major experimental problem with obtaining Raman spectra of zeolites with dispersive Raman spectroscopy is that zeolites tend to fluorescence when excited by the laser, which usually overwhelms the weaker Raman signal. However, with the introduction of Fourier Transform-Raman[107] and UV-Raman[108] spectrometers in recent years, fluorescence-free Raman spectra for most zeolite systems can be obtained. UV Raman spectroscopy employs UV excitation to minimize sample fluorescence by working away from the fluorescence spectral window. FT-Raman employs IR excitation that tends to minimize sample fluorescence.

Raman spectra of zeolites provide vibrational information about the zeolite structure and any additives introduced into the zeolites. Impregnation of metal oxide precursors into H-ZSM-5 zeolites, that are subsequently calcined, also leads to the formation of surface metal oxide species. The *in situ* Raman spectrum of dehydrated supported 3% V_2O_5/ZSM-5 (Si/Al = 15) is presented in Fig. 15 and exhibits Raman bands at 1038, 810, ∼525, 475, 378 and 293 cm^{-1}. The Raman bands at 810 (Si–O–Si), ∼525 (four-membered SiO_2 rings), and 475 cm^{-1} (five-membered SiO_2 rings) and ∼400 cm^{-1} (six-membered SiO_2 rings) are from the ZSM-5 zeolite support. The Raman vibrations at 1038 (v_s), 378 (δ) and 293 (δ V–O–Al) cm^{-1} are from the mono-oxo surface O=VO$_3$ species. The surface VO_4 species must be anchored to the H-ZSM-5 AlO$_x$ sites, with at least one V–O–Al bond, since crystalline V_2O_5 nanoparticles form for ZSM-5 zeolites with high Si/Al ratios (>200). Thus, surface metal oxide species readily react with the Al–(OH)–Si surface hydroxyls present in zeolites to form atomically dispersed metal oxide species that are often the catalytic active sites in zeolite-supported metal oxide catalysts.

Catalyst synthesis

There are an increasing number of Raman studies being reported during catalyst preparation appearing in the
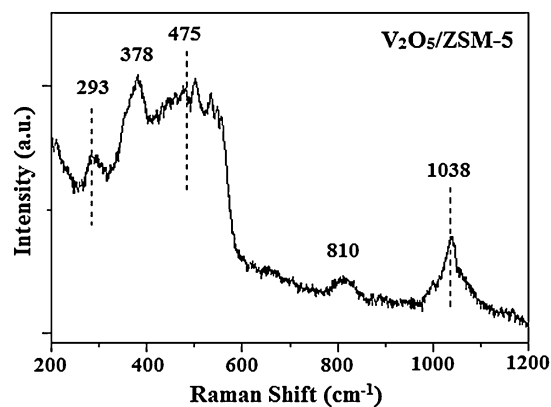
Fig. 15 *In situ* Raman spectrum (visible 532 nm) of dehydrated supported 3% V_2O_5/ZSM-5 (Si/Al = 15) under oxidizing conditions at 450 °C.

catalysis literature. Such vibrational measurements provide molecular level information about oxide species present in the precursor solution and crystalline oxide phases, even for XRD amorphous nanoparticles less than 4 nm.

Aqueous solutions of mixed oxides

A wealth of Raman literature has been published on the aqueous solution chemistry of pure molybdenum, vanadium, and tungsten polyoxometallates.[109–125] The Raman spectra of solutions containing molybdenum, tungsten and vanadium ions as a function of pH has been reported by Mestl and coworkers.[126–128] At high pH values of 6–9, Raman bands from aqueous, isolated MoO_4^{2-}, WO_4^{2-} and VO_4^{3-} species are present. Upon lowering the pH values, aqueous $Mo_7O_{24}^{6-}$, WO_x, $V_{10}O_{28}^{6-}$ clusters coexist. This is in line with the trends reported by Deo and Wachs on the role of pH for liquid-phase chemistry of transition metal salts.[45] At the pH value of 1, the bands of the pure polyoxometallates are replaced by those of the mixed polyoxometallate species.

Raman spectra revealed that aqueous $Al(OH)_4$ species polymerize into aluminosilicates that are the nuclei for crystal growth.[129] Raman spectra during synthesis of ZSM-5 show that the tetrapropylammonium template is initially trapped in the amorphous silica phase.[130–133] A comprehensive review about the genesis of zeolites being tracked by Raman spectroscopy has been collected by Mestl and Knozinger.[134]

Bulk V–P–O catalysts pass through various synthesis stages and also undergo further transformations on stream during the catalytic reaction.[135–139] The phase transformations in mesostructured V–P–O phases during thermal treatment in N_2 were monitored by Raman spectroscopy.[140] Raman spectra successfully monitored the progressive decomposition of the surfactant,[140] with two new Raman bands (∼1350 and ∼1590 cm^{-1}) appearing as the treatment temperature increased. These Raman bands are characteristic of graphite-like carbon species, which were generated from occluded surfactant molecules. The absence of second-order Raman spectra of the carbonaceous deposits in the wavenumber range of 2700–3200 cm^{-1} emphasizes the lack of long-range order in these carbonaceous aggregates.[141–143]

A critical stage of any catalyst preparation method is the formation of the catalytic active phase. Vanadium antimonate catalysts for propane ammoxidation are activated in the initial reaction period on stream. *Operando* Raman–GC analyses shows that catalysts initially consisting of surface vanadia and antimony oxide species on an Al_2O_3 support combine to form the bulk $VSbO_4$ (rutile) phase only during the ammoxidation reaction conditions.[144]

Hyphenated Raman spectroscopic techniques

Hyphenated spectroscopic methods involve combining Raman spectroscopy with other spectroscopic techniques or detectors. Raman spectroscopy can be combined with other spectroscopic probes such as IR, UV-vis, EPR, NMR, and XAS (XANES and EXAFS) and Temperature Programmed Surface Reaction (TPSR) spectroscopy to provide complementary catalyst fundamental information. For example, the vibrational selection rules for Raman–IR

spectroscopy are complementary, which allows for better assignment of the observed vibrations. Raman–UV-vis spectroscopy combines vibrational information with electronic information (oxidation state and domain size). Raman–EPR spectroscopy provides vibrational and local structures of paramagnetic species (V^{4+}, Cr^{5+}, Cr^{3+}, Mo^{5+}, W^{5+}, etc.). Combination of Raman spectroscopy with TPSR spectroscopy is denoted as Raman–TPSR spectroscopy and provides fundamental molecular structure-reactivity/selectivity relationships of catalytic active sites for all reactions. These hyphenated Raman techniques can also be performed with MS, IR or GC online product analysis and are referred to as *operando* Raman–MS, Raman–IR or Raman–GC spectroscopy, which was mentioned earlier.[38] However, these combinations alone do not fall into the hyphenated techniques category as they do not employ multiple spectroscopic techniques.

The current trend in hyphenated Raman techniques is to combine Raman with multiple spectroscopic techniques (IR, UV-vis, EPR and XAS). Brückner *et al.* reported the combination of EPR, Raman and UV-vis spectroscopy for the catalytic oxidative dehydrogenation of propane to propene over supported V_2O_5/TiO_2 catalysts.[145,146] Lin *et al.* combined Raman–IR spectroscopy to investigate metal–support interactions of Al_2O_3, SiO_2 and CeO_2-supported Pt catalysts in oxidizing and reducing conditions.[147] Zhao and Wachs employed Raman–IR–TPSR spectroscopy to investigate the surface reaction intermediates, reaction mechanism and the state of the catalytic active surface VO_x sites for propylene oxidation over supported V_2O_5/Nb_2O_5 with the aid of isotopically labeled $^{18}O_2$ (see Fig. 10 above).[86] It was demonstrated that the most abundant surface reaction intermediate is surface allyl ($C_3H_5^*$) species, the rate-determining-step involved cleavage of the surface allyl terminal C–H bond, the catalytic active surface VO_x sites are fully oxidized under reaction conditions, and lattice ^{16}O is involved in oxygen insertion into the surface $C_3H_5^*$ intermediate in the formation of the acrolein ($H_2C{=}CHCHO$) product. Bentrup *et al.* employed simultaneous *in situ* wide- and small-angle X-ray scattering (WAXS/SAXS) with Raman spectroscopy and combined Raman, attenuated total reflectance (ATR)-IR, and UV-vis spectroscopy to investigate the synthesis of molybdate catalyst precursors in aqueous solution.[148] The combination of Raman and diffuse reflectance infrared Fourier transform spectroscopy (DRIFTS) was applied to investigate NO_x storage catalysts over supported Pt–BaO/CeO_2 catalysts and demonstrated that more reliable identification and band assignments of the relevant surface and bulk processes could be obtained.[149]

In 2003, Weckhuysen published a state-of-the-art review of *in situ* spectroscopic characterization of catalysts that emphasized the benefits of employing combined *operando* spectroscopic techniques and laid the groundwork for future fundamental research studies of heterogeneous catalysis.[150] Tinnemans *et al.* combined Raman with UV-vis to develop a method that quantifies the Raman signal intensity from deposited coke on catalysts and applied the method to propane dehydrogenation over supported CrO_x/Al_2O_3

catalysts.[151,152] Beale *et al.* also studied propane dehydrogenation using combined Raman/UV-vis and XAFS to study the deactivation mechanism of supported MoO_x catalysts.[153]

It can be seen from the above review of *in situ* hyphenated Raman spectroscopy techniques that many combinations are possible as long as the secondary spectroscopic instrument can also be coupled with a reaction cell that allows for simultaneous collection of real-time spectroscopic data. The strong interest in applying hyphenated Raman techniques has already spawned several commercial optical spectrometers that combine Raman with IR and UV-vis.[154,155] In parallel to the development of hyphenated Raman techniques, there is also a strong effort to decrease the collection times for time-resolved measurements.[156,157] Though many of these studies feature "home made" reaction cells, the demand for combining techniques has also led to commercial availability of cells designed with multiple, simultaneous spectroscopies in mind.[158,159] Furthermore, the design of the cells is constantly being pushed to better mimic conventional fixed-bed reactor conditions and facilitate product analysis (*i.e.* low dead-volume, plug flow, absence of temperature gradients, and heated inlet and outlet streams).

Operando Raman spectroscopy

Recall that *operando* Raman spectroscopy is defined as simultaneous *in situ* Raman spectroscopic observation of the catalyst and online reaction product analysis (*e.g.*, MS, IR, GC, *etc.*) under relevant reaction conditions. The number of *operando* Raman spectroscopy studies reported to date in the catalysis literature are still rather limited (see Fig. 1). Given that the concept of *operando* Raman spectroscopy was only recently well defined in the literature in 2002,[5,38,60,144] that is not unexpected. To date, a search of the literature for "*operando* Raman" yielded only 42 publications (though the methodology precedes the terminology).[160,161] A significant portion of these publications has been to demonstrate that performing *in situ* spectroscopic studies with on-line, real-time product analysis is feasible and provide new fundamental insights not previously achievable with *in situ* spectroscopy studies. These publications could be considered an effort to show the catalysis community that *operando* spectroscopy implementation has become feasible and facile. Many of the combined techniques described in the above hyphenated Raman spectroscopic techniques section also implemented *operando* spectroscopy capabilities and the reader is referred to that section of the review and the indicated references.[86,145–148,150–153] The reader is also referred to the instrument vendors listed in the hyphenated Raman section for information on the instruments being utilized to perform *operando* Raman spectroscopy.[154,155,158,159]

Given the relative infancy of this experimental methodology, an amazing amount of knowledge has been gained from the *operando* spectroscopy studies to date. The most frequently investigated reaction has been methanol oxidation over various catalysts. For supported MoO_3/Al_2O_3 catalysts, Brandhorst *et al.* used combined Raman–IR with online GC product analysis.[162] The simultaneous use of complementary detectors allowed for observation of the surface intermediates

by IR and surface Mo–OH species by Raman, and their formation/disappearance was correlated with methanol conversion to formaldehyde, methyl formate and dimethyl ether. Other *operando* Raman spectroscopy methanol oxidation studies have been performed on a wide range of catalytic materials: Ag,[163] supported MoO_x/SiO_2,[164] supported MoO_x/TiO_2,[165] supported VO_x/SiO_2,[166] and supported Rh/TiO_2.[167] This selection of catalytic materials demonstrates the ability of the *operando* spectroscopy methodology to be applied to everything from bulk metals to mixed metal oxides.

The array of possible materials is further broadened when looking at the *operando* Raman studies focusing on hydrocarbon oxidation. Arendt *et al.* employed Raman with online GC product analysis to study a Wells–Dawson salt $((NH_4)_6P_2Mo_{18}O_{62})$ and phosphomolybdate Keggin structures $(H_3PMo_{12}O_{40}$ and $(NH_4)_3PMo_{12}O_{40})$ for propene oxidation.[168] Similarly, Loridant *et al.* combined Raman with online GC-MS product analysis to study selective oxidation of isobutane to methacrolein and methacrylic acid over phosphomolybdate Keggins with Ce, Te and V counter-cations.[169] This study even showed that a correlation between resonant Raman effects and selectivity to product formation could be developed by employing *operando* spectroscopy.

With regards specifically to the determination of the catalytic active sites in a catalytic process, the reader is again referred to the Weckhuysen review.[150] *Operando* Raman spectroscopy has been shown to be able to elucidate the nature of the catalytic active sites for numerous catalytic materials and reactions. *Operando* Raman–GC was employed for the examination of propane ammoxidation over supported VO_x–SbO_x/Al_2O_3 catalysts to elegantly demonstrate that the surface VO_x–SbO_x phase transforms to the catalytic active crystalline $SbVO_4$ nanoparticles under the ammoxidation reaction conditions.[144] Similarly, Guerrero-Perez *et al.* investigated supported V–Mo–W–O/Al_2O_3 catalysts during oxidative dehydrogenation of propane to determine how to specifically improve selectivity to propylene.[170] By identifying the Mo–W–O and V–W–O as the phases giving better propylene yields, it was demonstrated that the catalyst performance can be improved by making tungsten oxide the majority component of the catalyst formulation. The ability to simultaneously monitor the catalytic active phase of such complex, multi-phase supported metal oxide catalysts and obtain real-time selectivity data facilitated the rational design of an improved catalyst.

Operando Raman spectroscopy can not only determine the active phase of a catalyst, but it can also assist in pin pointing the exact catalytic active site involved in the reaction. In the *operando* Raman–GC study of oxidative dehydrogenation of ethane over supported MoO_x/Al_2O_3 catalysts, Christodoulakis *et al.* were able to develop structure–activity relationships between the surface MoO_x species and the catalytic activity and selectivity performance.[171] A direct correlation between the number bridging Mo–O–Al bonds and the turnover frequency (TOF) of the ethane ODH reaction was demonstrated. It was, thus, concluded that the bridging Mo–O–Al bond is the catalytic active site for this catalyst system rather than the terminal Mo=O or bridging

Mo–O–Mo bonds. While such conclusions about the exact catalytic active site may be conjectured without the application of the *operando* Raman spectroscopy methodology, only *operando* Raman spectroscopy studies can directly establish fundamental structure–activity/selectivity relationships.

Recently, high-throughput *operando* Raman spectroscopy systems have been reported that are able to simultaneously monitor as many as six parallel catalysts with each catalytic reactor having its own online analysis of reaction products.[166,166] Such high-throughput *operando* Raman systems should be attractive to industrial laboratories that wish to simultaneously screen multiple catalysts for the same reaction.

In its relatively short period, *operando* Raman spectroscopy has made a significant impact in the catalysis world, especially with regards to determination of the active phase and/or site. The benefits of the methodology undoubtedly are the reason for the thrust in implementation. (1) Recent developments in commercially available instrumentation (spectrometers and reaction cells) have made implementation more facile. (2) The ability to do Raman spectroscopy under a wide range of temperatures, in many environments, and on many materials is extended to the *operando* case. (3) The molecular nature of Raman spectroscopy is also taken advantage of during *operando* studies, allowing insight into the active phase under real reaction conditions. (4) The development of structure–activity relationships due to the collection of real-time catalytic activity and selectivity data can lead to the elucidation of the exact active site, and can ultimately facilitate the rational design of improved catalytic materials.

Quantitative Raman spectroscopy

Although Raman spectroscopy is not inherently quantitative because of its non-linear response to color changes of the catalysts as a function of composition and reaction conditions, it is still possible to perform quantitative Raman spectroscopy when an internal standard is present. Fortunately, many supported catalysts the oxide support possesses Raman active modes (*e.g.*, SiO_2, ZrO_2, TiO_2, *etc.*) that allow the spectra to be normalized against the support Raman band. For example, the vibration of the ZrO_2 support was employed as an internal standard to determine the coverage of surface WO_x species.[172] It was demonstrated that the surface WO_x vibration continuously increased with tungsten oxide loading until monolayer coverage was achieved and remained constant afterwards. At which point, the Raman bands for crystalline WO_3 linearly increased with further tungsten oxide coverage. Sometimes, however, it may be necessary to introduce an internal standard since the support may not give Raman active modes (*e.g.*, transitional alumina phases and ionic materials).[29]

Tinnemans *et al.* have also shown that using an *operando* hyphenated technique (Raman–UV-vis) makes it possible to obtain quantitative Raman spectra without the need of an internal standard.[151] By using a relationship between the diffuse reflectance of the catalytic solid of infinite thickness and the Raman intensity, they were able to apply a UV-vis correction factor to obtain quantification of the amount of

5014 | *Chem. Soc. Rev.*, 2010, **39**, 5002–5017

This journal is © The Royal Society of Chemistry 2010

coke formed in a propane dehydrogenation fixed-bed reactor as a function of catalyst bed height and reaction time for supported 13% Cr/Al_2O_3. Thus, it is possible to obtain quantitative Raman spectra for most heterogeneous catalytic systems when internal standards are present and even without them when UV-vis measurements are possible.

Advantages and disadvantages of Raman spectroscopic characterization of catalysts

The advantages of Raman spectroscopy have been enumerated above and it is also important to point out some of its potential disadvantages. As already indicated, sample fluorescence can occasionally be a problem, especially with zeolites and layered hydroxides, when employing visible excitation. Care must also be taken to make sure that no photochemistry is initiated by the laser excitation on the surface reaction intermediates and the catalyst. This is usually not a significant problem with the low laser powers currently employed and can be easily minimized by rotating the catalyst, rastering the laser beam over the sample or even fluidizing the catalyst particles. Although UV excitation significantly minimizes sample fluorescence, the much higher energy content of the UV source can lead to significant photochemistry under certain conditions. This does not seem to be much of an issue with UV excitation at 325 nm, but does become a significant issue with deep UV excitation at 244 nm where the laser excitation can both reduce the catalyst and decompose the surface reaction intermediates and reactants. The disadvantage of FT-Raman is that the signals of the surface MO_x species (e.g., MoO_x, VO_x, WO_x. etc.) are extremely weak and the spectra are mostly dominated by the crystalline components (e.g., MoO_3, V_2O_5, WO_3, etc.). Furthermore, it is not possible to perform in situ studies with FT-Raman spectroscopy above $\sim 150\,^{\circ}C$ because of sample emission in the IR region at elevated temperatures. This serious limitation of FT-Raman spectroscopy, unfortunately, prevents FT-Raman from performing cutting edge in situ studies of heterogeneous catalysts.

As demonstrated by the high-temperature UV Raman spectroscopy studies in this review (see Fig. 8 and 9), temperature is no longer a limitation to collecting Raman spectra at extreme reaction temperatures. With the ability of UV Raman spectroscopy to collect radiation emission-free spectra at extreme temperatures, the only limitation becomes the temperature limits of the in situ environmental cell and the thermal stability of the lenses used to collect the scattered Raman light from the hot catalysts. Although the reported Raman studies of heterogeneous catalysts are almost exclusively collected at atmospheric pressure, there is no pressure limitation to Raman spectroscopy as long as the environmental cell is designed to maintain high pressure environments. Very high pressure Raman spectroscopy studies can be found in geologic studies where pressures simulating those found within the earth's crust are recreated using diamond-anvil cells. Sharma et al. used in situ Raman to study methanogenesis at these extreme pressures and temperatures.[173] They reported Raman spectra at pressures of $\sim 5.5 \pm 0.5$ GPa $(\sim 5.4 \times 10^4 \pm 4.9 \times 10^3$ atm) and at temperatures greater than 1000 °C.

In summary, visible and UV Raman spectroscopy have shown to be the most productive Raman spectroscopic methods for the study of heterogeneous catalysts.

Conclusions

The molecular aspect of the Raman vibrational selection rules allows for the molecular structural and reactivity determinations of metal oxide catalytic active sites in all types of oxide catalyst systems (supported metal oxides, zeolites, layered hydroxides, polyoxo metallates (POMs), bulk pure metal oxides, bulk mixed oxides and mixed oxide solid solutions) with in situ Raman spectroscopy under all environmental conditions (aqueous, hydrated, dehydrated and reactive environments). The metal oxide catalytic active sites' molecular structural and reactivity determinations are greatly facilitated by the use of isotopically labeled molecules. The ability of Raman spectroscopy to (1) operate in all phases (liquid, solid, gas and their mixtures), (2) operate over a very wide temperature (-273 to $> 1000\,^{\circ}C$) and pressure (UHV to $\gg 100$ atm), and (3) provide molecular level information about metal oxides makes Raman spectroscopy the most informative characterization technique for understanding the molecular structure and surface chemistry of metal oxide catalytic active sites in heterogeneous catalysis. The recent use of hyphenated Raman spectroscopy instrumentation and operando Raman spectroscopy methodology is allowing for the establishment of direct structure–activity/selectivity relationships that will have a significant impact on catalysis science in this decade. Consequently, the growth in the use of Raman spectroscopy in heterogeneous catalysis research is poised to continue to exponentially grow in the coming years.

Acknowledgements

References

1 K. Nakamoto, Infrared and Raman Spectra of Inorganic and Coordination Compounds, Part A and Part B, John Wiley & Sons, Hoboken, 2009.
2 J. C. Lavalley, Catal. Today, 1996, 27, 377.
3 I. E. Wachs, Catal. Today, 1996, 27, 437; I. E. Wachs, Catal. Today, 2005, 100, 79.
4 G. Busca, J. Raman Spectrosc., 2002, 33, 348.
5 G. Mestl, J. Mol. Catal. A: Chem., 2000, 158, 45; I. E. Wachs, in Handbook of Raman Spectroscopy, Practical Spectroscopy, Marcel Dekker, New York, 2001, vol. 28, p. 799; M. A. Banares, in In situ Spectroscopy of Catalysts, ed. B. M. Weckhuysen, American Scientific Publishers, Stevenson Ranch, CA, 2004, p. 59; M. A. Banares and I. E. Wachs, J. Raman Spectrosc., 2002, 33, 359; M. A. Banares and G. Mestl, Adv. Catal., 2009, 52, 43; M. A. Banares and I. E. Wachs, Encyclopedia of Analytical Chemistry, ed. R. A. Meyers, Wiley, Hoboken, 2010, p. a9034.
6 F. R. Brown, L. E. Makovsky and H. K. Rhee, Appl. Spectrosc., 1977, 31, 563.
7 R. J. Thomas, J. A. Moulijn and F. P. J. M. Kerkhof, Recl. Trav. Chim. Pays-Bas, 1977, 96, M114; F. P. J. M. Kerkhof, J. A. Moulijn and R. J. Thomas, J. Catal., 1979, 56, 279.
8 H. Knozinger and H. Jeziorowski, J. Phys. Chem., 1978, 82, 2002; H. Jeziorowski, J. Phys. Chem., 1979, 83, 1166.

9 F. Roozeboom, J. Medema and P. J. Gellings, *Z. Phys. Chem.*, 1978, **111**, 215.

10 A. Iannibello, P. L. Villa and S. Marengo, *Gazz. Chim. Ital.*, 1979, **109**, 521.

11 C. P. Cheng, J. D. Ludowise and G. L. Schrader, *Appl. Spectrosc.*, 1980, **34**, 146.

12 E. Payen, M. C. Dhamelincourt, P. Dhamelincourt, J. Grimblot and J. P. Bonelle, *Appl. Spectrosc.*, 1982, **36**, 30.

13 L. Wang and W. K. Hall, *J. Catal.*, 1980, **66**, 251; L. Wang and W. K. Hall, *J. Catal.*, 1983, **82**, 177.

14 G. L. Schrader and C. P. Cheng, *J. Catal.*, 1983, **80**, 369.

15 S. S. Chan, I. E. Wachs, L. L. Murrell, L. Wang and K. Hall, *J. Phys. Chem.*, 1984, **88**, 5831.

16 J. M. Stencel, L. E. Makovsky, T. A. Sarkus, J. De Vries, R. Thomas and J. A. Moulijn, *J. Catal.*, 1984, **90**, 314.

17 S. S. Chan and A. T. Bell, *J. Catal.*, 1984, **89**, 433.

18 Y. Okamoto and T. Imanaka, *J. Phys. Chem.*, 1988, **92**, 7102.

19 J. M. Stencel, J. R. Diehl, J. R. D'Este, L. E. Makowsky, L. Rodrigo, K. Marcinkowska, A. Adnot, P. C. Roberge and S. Kaliaguine, *J. Phys. Chem.*, 1986, **90**, 4739.

20 S. S. Chan and I. E. Wachs, *J. Catal.*, 1987, **103**, 224.

21 F. D. Hardcastle and I. E. Wachs, *J. Phys. Chem.*, 1988, **46**, 173.

22 J. Leyrer, D. Mey and H. Knozinger, *J. Catal.*, 1990, **124**, 349.

23 J.-M. Jehng and I. E. Wachs, *J. Phys. Chem.*, 1991, **95**, 7373.

24 M. A. Vuurman and I. E. Wachs, *J. Phys. Chem.*, 1992, **96**, 5008.

25 G. J. Hutchings, A. Desmartin-Chomel, R. Olier and J. C. Volta, *Nature*, 1994, **368**, 41.

26 J. H. Lunsford, X. Yang, K. Haller, J. Laane, G. Mestl and H. Knozinger, *J. Phys. Chem.*, 1993, **97**, 13810.

27 M. A. Banares, N. D. Spencer, M. D. Jones and I. E. Wachs, *J. Catal.*, 1994, **146**, 204.

28 M. A. Banares, H. Hu and I. E. Wachs, *J. Catal.*, 1995, **155**, 249.

29 H. Hu and I. E. Wachs, *J. Phys. Chem.*, 1995, **99**, 10911; H. Hu, S. R. Bare and I. E. Wachs, *J. Phys. Chem.*, 1995, **99**, 10897.

30 J.-M. Jehng, H. Hu, X. Gao and I. E. Wachs, *Catal. Today*, 1996, **28**, 335.

31 I. E. Wachs, G. Deo, B. M. Weckhuysen, A. Andreini, M. A. Vuurman, M. de Boer and M. D. Amiridis, *J. Catal.*, 1996, **161**, 211.

32 I. E. Wachs, J.-M. Jehng, G. Deo, B. M. Weckhuysen, V. Guliants and J. B. Benziger, *Catal. Today*, 1996, **32**, 47.

33 B. M. Weckhuysen and I. E. Wachs, *J. Phys. Chem.*, 1996, **100**, 14437.

34 I. E. Wachs, J.-M. Jehng, G. Deo, B. M. Weckhuysen, V. V. Guliants, J. B. Benziger and S. Sundaresan, *J. Catal.*, 1997, **170**, 75.

35 X. Gao, J. L. G. Fierro and I. E. Wachs, *Langmuir*, 1999, **15**, 3169.

36 C.-B. Wang, G. Deo and I. E. Wachs, *J. Phys. Chem. B*, 1999, **103**, 5645.

37 M. A. Banares, M. V. Martinez-Huerta, X. Gao, J. L. G. Fierro and I. E. Wachs, *Catal. Today*, 2000, **61**, 295.

38 B. M. Weckhuysen, *Chem. Commun.*, 2002, 97; M. O. Guerrero-Perez and M. A. Banares, *Chem. Commun.*, 2002, 1292; M. A. Banares, *Catal. Today*, 2005, **100**, 71.

39 C. Baes and R. E. Messmer, *Hydrolysis of Cations*, John Wiley & Sons, New York, 1976, p. 258.

40 D. S. Kim, K. Segawa, T. Soeya and I. E. Wachs, *J. Catal.*, 1992, **136**, 539.

41 J. A. Bergwerff, T. Visser and B. M. Weckhuysen, *Catal. Today*, 2008, **130**, 117.

42 J. A. Bergwerff, T. Visser, B. R. G. Leliveld, B. D. Rossenaar, K. P. de Jong and B. M. Weckhuysen, *J. Am. Chem. Soc.*, 2004, **126**, 14548.

43 J. A. Bergwerff, M. Jansen, B. R. G. Leliveld, T. Visser, K. P. de Jong and B. M. Weckhuysen, *J. Catal.*, 2006, **243**, 292.

44 J. E. Molinari and I. E. Wachs, *J. Am. Chem. Soc.*, 2010, **132**, 12559.

45 G. Deo and I. E. Wachs, *J. Phys. Chem.*, 1991, **95**, 5889.

46 C. Rocchiccioli-Deltcheff, M. Amirouche, M. Che, J. M. Tatibouet and M. Fournier, *J. Catal.*, 1990, **125**, 2892.

47 X. Carrier, J. F. Lambert and M. Che, *J. Am. Chem. Soc.*, 1997, **119**, 10137.

48 L. Le Bihan, P. Blanchard, M. Fournier, J. Grimblot and E. Payen, *J. Chem. Soc., Faraday Trans.*, 1998, **94**, 937.

49 E. L. Lee and I. E. Wachs, *J. Phys. Chem. C*, 2007, **111**, 14410.

50 S. Chempath, Y. Zhang and A. T. Bell, *J. Phys. Chem. C*, 2007, **111**, 1291.

51 J. Handzlik, *Chem. Phys. Lett.*, 2009, **469**, 140.

52 J. Handzlik and P. Sautet, *J. Phys. Chem. C*, 2008, **112**, 14456.

53 H. Tian, C. A. Roberts and I. E. Wachs, *J. Phys. Chem. C*, 2010, **114**, 14110.

54 C. Cristiani, P. Forzatti and G. Busca, *J. Catal.*, 1989, **116**, 586.

55 G. T. Went, S. T. Oyama and A. T. Bell, *J. Phys. Chem.*, 1990, **94**, 4240.

56 U. Scharf, M. Schraml-Marth, M. Wokaun and A. Baiker, *J. Chem. Soc., Faraday Trans.*, 1991, **87**, 3299.

57 G. T. Went, L.-J. Leu, R. Rosin and A. T. Bell, *J. Catal.*, 1992, **134**, 479.

58 N. Das, H. Eckerdt, H. Hu, I. E. Wachs, J. F. Walzer and F. Feher, *J. Phys. Chem.*, 1993, **97**, 8240.

59 X. Gao, S. R. Bare, B. M. Weckhusyen and I. E. Wachs, *J. Phys. Chem. B*, 1998, **102**, 10842.

60 M. O. Guerrero-Perez and M. A. Banares, *Chem. Commun.*, 2002, 1292; M. A. Banares, M. O. Guerrero-Perez, G. Garcia-Cortez and J. L. G. Fierro, *J. Mater. Chem.*, 2002, **12**, 3337; M. O. Guerrero-Perez and M. A. Banares, *Catal. Today*, 2004, **96**, 265.

61 D. E. Keller, F. M. de Groot, D. C. Koningsberger and B. M. Weckhuysen, *J. Phys. Chem. B*, 2005, **109**, 10223.

62 N. Magg, B. Immaraporn, J. B. Giorgi, T. Schroeder, M. Baumer, J. Dobler, Z. Wu, E. Kondratenko, M. Cherian, M. Baerns, P. C. Stair, J. Sauer and H. J. Freund, *J. Catal.*, 2004, **226**, 88.

63 J. Bronkma and A. T. Bell, *J. Phys. Chem. C*, 2007, **111**, 420.

64 Z. Wu, S. Dai and S. H. Overbury, *J. Phys. Chem. C*, 2010, **114**, 412.

65 R. M. Pittman and A. T. Bell, *J. Phys. Chem.*, 1993, **97**, 12178.

66 L. J. Burcham, J. Datka and I. E. Wachs, *J. Phys. Chem. B*, 1999, **103**, 6015.

67 X. Gao, I. E. Wachs, M. S. Wong and J. Y. Ying, *J. Catal.*, 2001, **203**, 18.

68 M. Baltes, A. Kytokivi, B. M. Weckhuysen, R. A. Schoonheydt, P. van der Voort and E. F. Vansant, *J. Phys. Chem. B*, 2001, **105**, 6211.

69 Y. Chen, J. L. G. Fierro, T. Tanaka and I. E. Wachs, *J. Phys. Chem. B*, 2003, **107**, 5243.

70 M. A. Vuurman and I. E. Wachs, *J. Mol. Catal.*, 1993, **84**, 193.

71 J.-M. Jehng, I. E. Wachs, B. M. Weckhuysen and R. A. Schoonheydt, *J. Chem. Soc., Faraday Trans.*, 1995, **91**, 953.

72 T. J. Dines and S. Inglis, *Phys. Chem. Chem. Phys.*, 2003, **5**, 1320.

73 E. Groppo, A. Damin, F. Bonino, A. Zecchina, S. Bordiga and C. Lamberti, *Chem. Mater.*, 2005, **17**, 2019; E. Groppo, C. Lamberti, S. Bordiga, G. Spoto and A. Zecchina, *Chem. Rev.*, 2005, **105**, 115.

74 C. Moisii, W. Deguns, A. Lita, S. D. Callahan, L. J. van de Burgt, D. Magana and A. E. Stiegman, *Chem. Mater.*, 2006, **18**, 3965; C. Moisii, M. D. Curran, L. J. van de Burgt and A. E. Stiegman, *J. Mater. Chem.*, 2005, **15**, 3519.

75 R. Radhakrishnan, C. Reed, S. T. Oyama, M. Seman, J. N. Kondo, K. Domen, Y. Ohminami and K. Asakura, *J. Phys. Chem. B*, 2001, **105**, 8519.

76 N. Ohler and A. T. Bell, *J. Phys. Chem. B*, 2005, **109**, 23419.

77 D. S. Kim, M. Ostromecki and I. E. Wachs, *J. Mol. Catal. A: Chem.*, 1996, **106**, 93.

78 M. Scheithauer, R. K. Grasselli and H. Knozinger, *Langmuir*, 1998, **14**, 3019; M. Scheithauer, T.-K. Cheung, R. E. Jentoft, R. K. Grasselli, B. C. Gates and H. Knozinger, *J. Catal.*, 1998, **180**, 1.

79 D. G. Barton, S. L. Soled, G. D. Meitzner, G. A. Fuentes and E. Iglesia, *J. Catal.*, 1999, **181**, 57.

80 T. Kim and I. E. Wachs, *J. Catal.*, 2007, **246**, 370.

81 E. I. Ross-Medggarden and I. E. Wachs, *J. Phys. Chem. C*, 2007, **111**, 15089.

82 H. Nair and C. D. Baertsch, *J. Catal.*, 2008, **258**, 1.

83 M. A. Vuurman, D. J. Stufkens, A. Oskan and I. E. Wachs, *J. Mol. Catal.*, 1992, **76**, 263.

84 S. S. Chan, I. E. Wachs, L. L. Murrell and N. C. Dispenziere, Jr., *J. Catal.*, 1985, **92**, 1.

85 J. M. Thomas and W. J. Thomas, *Principles and Practice of Heterogeneous Catalysis*, VCH Verlagsgesellschaft mbH, Weinheim, 1997.

86 C. Zhou and I. E. Wachs, *J. Phys. Chem. C*, 2008, **112**, 11363.

87 B. M. Weckhuysen, J.-M. Jehng and I. E. Wachs, *J. Phys. Chem. B*, 2000, **104**, 7382.

5016 | *Chem. Soc. Rev.*, 2010, **39**, 5002–5017

This journal is © The Royal Society of Chemistry 2010

88 E. L. Lee and I. E. Wachs, *J. Phys. Chem. C*, 2008, **112**, 6487.
89 A. F. Wells, *Structural Inorganic Chemistry*, Oxford University, London, 1984.
90 J.-M. Jehng and I. E. Wachs, *Chem. Mater.*, 1991, **3**, 100.
91 H. H. Brongersma, M. Draxler, M. de Ridder and P. Bauer, *Surf. Sci. Rep.*, 2007, **62**, 63.
92 Z. Zhao, X. Gao and I. E. Wachs, *J. Phys. Chem. B*, 2003, **107**, 6333.
93 G. Mestl, *J. Raman Spectrosc.*, 2002, **33**, 333.
94 O. Ovsitser, Y. Uchida, G. Mestl, G. Weinberg, A. Blume, J. Jager, M. Dieterle, H. Hibst and R. Schlogl, *J. Mol. Catal. A: Chem.*, 2002, **185**, 291.
95 S. Knobl, G. A. Zenkovets, G. N. Kryukova, O. Ovsitser, D. Niemeyer, R. Schlogl and G. Mestl, *J. Catal.*, 2003, **215**, 177.
96 G. A. Tsigdinos, *Top. Curr. Chem.*, 1978, **76**, 1.
97 N. Mizuno, W. Hann and T. Kudo, *J. Catal.*, 1998, **178**, 391.
98 T. Okuhara, N. Mizuno and M. Misono, *Adv. Catal.*, 1996, **41**, 113.
99 H. Liu and E. Iglesia, *J. Phys. Chem. B*, 2003, **107**, 10840.
100 L. Nakka, J. E. Molinari and I. E. Wachs, *J. Am. Chem. Soc.*, 2009, **131**, 15544.
101 J. Twu and P. K. Datta, *J. Catal.*, 1990, **124**, 503.
102 K. Lee, M. Beaver, H. Caram and S. Sircar, *Ind. Eng. Chem. Res.*, 2008, **47**, 8048.
103 W. Kagunya, R. Baddour-Hadjean, F. Kooli and W. Jones, *Chem. Phys.*, 1998, **236**, 225; L. Hickey, J. Kloprogge and R. Frost, *J. Mater. Sci.*, 2000, **35**, 4347; J. Kloprogge, D. Wharton, L. Hickey and R. Frost, *Am. Mineral.*, 2002, **87**, 623; H. Du, C. Williams, A. Ebner and J. Ritter, *Chem. Mater.*, 2010, **22**, 3519.
104 C. Bremard and D. Bougeard, *Adv. Mater.*, 1995, **7**, 10.
105 P.-P. Knops-Gerrits, D. E. De Vos, E. J. P. Feijen and P. A. Jacobs, *Microporous Mater.*, 1997, **8**, 3.
106 I. E. Wachs, in *Handbook of Raman Spectroscopy*, ed. I. R. Lewis, H. G. M. Edwards, Marcel Dekker, New York, 2001, p. 799.
107 Y. Huang, R. R. Poissant and P. Qiu, *Langmuir*, 2000, **16**, 889.
108 P. C. Stair, *Adv. Catal.*, 2007, **51**, 75.
109 C. P. Cheng and G. L. Schrader, *J. Catal.*, 1979, **60**, 276.
110 F. Gonzales-Vilchez and W. P. Griffith, *J. Chem. Soc., Dalton Trans.*, 1972, 1449.
111 W. P. Griffith and P. J. B. Lesniak, *J. Chem. Soc. A*, 1969, 1066.
112 W. P. Griffith and T. D. Wickins, *J. Chem. Soc. A*, 1967, 675.
113 W. P. Griffith, *J. Chem. Soc. A*, 1970, 286.
114 S. Himeno, N. Niiya and T. Ueda, *Bull. Chem. Soc. Jpn.*, 1997, **70**, 631.
115 W. D. Hunnius, *Z. Naturforsch., Teil B*, 1975, **30**, 63.
116 G. Johansson, L. Pettersson and N. Ingri, *Acta Chem. Scand., Ser. A*, 1979, **33a**, 305.
117 K. Y. S. Ng and E. Gulari, *Polyhedron*, 1984, **3**, 1001.
118 G. L. Schrader, M. S. Basista and C. B. Bergman, *Chem. Eng. Commun.*, 1981, **12**, 121.
119 K. H. Tytko and O. Glemser, *Adv. Inorg. Chem. Radiochem.*, 1976, **19**, 239.
120 K. H. Tytko and J. Mehrnke, *Z. Anorg. Allg. Chem.*, 1983, **503**, 67.
121 K. H. Tytko and B. Schönfeld, *Z. Naturforsch., Teil B*, 1975, **30**, 471.
122 V. Cordis, K. H. Tytko and O. Glemser, *Z. Naturforsch., Teil B*, 1975, **30**, 834.
123 K. H. Tytko, G. Petridis and B. Schönfeld, *Z. Naturforsch., Teil B*, 1980, **35**, 45.
124 K. H. Tytko, G. Baethe, E. R. Hirschfeld, J. Mehrnke and D. Stellthorn, *Z. Anorg. Allg. Chem.*, 1983, **503**, 43.
125 J.-M. Jehng and I. E. Wachs, *J. Raman Spectrosc.*, 1991, **22**, 83.
126 M. Dieterle, G. Mestl, J. Jager, Y. Uchida and R. Schlogl, *J. Mol. Catal. A: Chem.*, 2001, **174**, 169.
127 S. Knobl, G. A. Zenkovets, G. N. Kryukova, O. Ovsitser, D. Niemeyer, R. Schlögl and G. Mestl, *J. Catal.*, 2003, **215**, 177.
128 G. J. Mestl, *J. Raman Spectrosc.*, 2002, **33**, 333.
129 F. Roozeboom, H. Robson and S. S. Chan, *Zeolites*, 1983, **3**, 321.
130 H. Baranska, B. Czerwinska and A. Labudzinska, *J. Mol. Struct.*, 1986, **143**, 485.
131 P. K. Dutta and M. Puri, *J. Phys. Chem.*, 1987, **91**, 4329.
132 P. K. Dutta and D. C. Shieh, *J. Phys. Chem.*, 1986, **90**, 2331.
133 P. K. Dutta, D. C. Shieh and M. Puri, *J. Phys. Chem.*, 1987, **91**, 2332.

134 G. Mestl and H. Knözinger, in *Handbook of Heterogeneous Catalysis*, ed. G. Ertl, H. Knözinger and J. Weitkamp, Wiley-VCH, Weinheim, 1997, vol. 2, p. 539.
135 F. B. Abdelouahab, R. Olier, N. Guilhaume, F. Lefebvre and J. C. Volta, *J. Catal.*, 1992, **134**, 151.
136 V. V. Guliants, J. B. Benziger, S. Sundaresan, N. Yao and I. E. Wachs, *Catal. Lett.*, 1995, **32**, 379.
137 V. V. Guliants, S. A. Holmes, J. B. Benziger, P. Heaney, D. Yates and I. E. Wachs, *J. Mol. Catal. A: Chem.*, 2001, **172**, 265.
138 G. J. Hutchings, A. Desmartin-Chomel, R. Olier and J. C. Volta, *Nature*, 1994, **368**, 41.
139 J. C. Volta, K. Bere, Y. J. Zhang and R. Olier, *ACS Symp. Ser.*, 1993, **523**, 217.
140 M. A. Carreón, V. V. Guliants, M. O. Guerrero-Pérez and M. A. Bañares, *Microporous Mesoporous Mater.*, 2004, **71**, 57.
141 K. Angoni, *J. Mater. Sci.*, 1998, **33**, 3693.
142 A. Cuesta, P. Dhamelincourt, J. Laureyns, A. Martínez-Alonso and J. M. D. Tascón, *Carbon*, 1994, **32**, 1523.
143 R. Vidano and D. B. Fischbach, *J. Am. Ceram. Soc.*, 1978, **61**, 13.
144 M. O. Guerrero-Pérez and M. A. Bañares, *Chem. Commun.*, 2002, 1292.
145 A. Bruckner, *Chem. Commun.*, 2005, 1761.
146 A. Bruckner and E. V. Kondratenko, *Catal. Today*, 2006, **113**, 16.
147 W. Lin, A. A. Herzing, C. J. Kiely and I. E. Wachs, *J. Phys. Chem. C*, 2008, **112**, 5942.
148 U. Bentrup, J. Radnik, U. Armbruster, A. Martin, J. Leiterer, F. Emmerling and A. Bruckner, *Top. Catal.*, 2009, **52**, 1350.
149 A. Urakawa, N. Maeda and A. Baiker, *Angew. Chem., Int. Ed.*, 2008, **47**, 9256.
150 B. M. Weckhuysen, *Phys. Chem. Chem. Phys.*, 2003, **5**, 4351.
151 S. J. Tinnemans, M. H. F. Kox, T. A. Nijhuis, T. Visser and B. M. Weckhuysen, *Phys. Chem. Chem. Phys.*, 2005, **7**, 211.
152 S. J. Tinnemans, J. G. Mesu, K. Kervinen, T. Visser, T. A. Nijhuis, A. M. Beale, D. E. Keller, A. M. J. van der Eerden and B. M. Weckhuysen, *Catal. Today*, 2006, **113**, 3.
153 A. M. Beale, A. M. J. van der Eerden, K. Kervinen, M. A. Newton and B. M. Weckhuysen, *Chem. Commun.*, 2005, 3015.
154 <www.horiba.com/scientific>.
155 <www.renishaw.com>.
156 AvaSpec-128 Ultrafast Fiber Optic Spectrometer, <www.avantes.com>.
157 Thermo Scientific Nicolet 8700 Research Spectrometer, <www.thermoscientific.com>.
158 Linkam CCR 1000, <www.linkam.co.uk>.
159 High Temperature Praying Mantis Reaction Chamber, <www.harricksci.com>.
160 I. E. Wachs, J.-M. Jehng, G. Deo, B. M. Weckhuysen, V. V. Guliants, J. B. Benziger and S. Sundaresan, *J. Catal.*, 1997, **170**, 75.
161 C.-B. Wang, G. Deo and I. E. Wachs, *J. Phys. Chem. B*, 1999, **103**, 5645.
162 M. Brandhorst, S. Cristol, M. Capron, C. Dujardin, H. Vezin, G. Le bourdan and E. Payen, *Catal. Today*, 2006, **113**, 34.
163 E. Cao, S. Firth, P. F. McMillan and A. Gavriilidis, *Catal. Today*, 2007, **126**, 119.
164 J.-F. Paul, K. Hamraoui, S. Cristol, A.-S. Mamede and E. Payen, *Stud. Surf. Sci. Catal.*, 2006, **172**, 377.
165 G. Li, D. Hu, G. Xia and Z. C. Zhang, *Top. Catal.*, 2009, **52**, 1381.
166 G. Li, D. Hu, G. Xia and Z. C. Zhang, *Top. Catal.*, 2010, **53**, 40.
167 X. Secordel, E. Berrier, M. Capron, S. Cristol, J.-F. Paul, M. Fournier and E. Payen, *Catal. Today*, 2010, **155**, 177.
168 E. Arendt, S. Ghislain and E. M. Gaigneaux, *Catal. Today*, 2010, **155**, 227.
169 S. Loridant, Q. Huynh and J.-M. M. Millet, *Catal. Today*, 2010, **155**, 214.
170 M. O. Guerrero-Pérez, M. C. Herrera, I. Malpartida, M. A. Larrubia, L. J. Alemany and M. A. Bañares, *Catal. Today*, 2007, **126**, 177.
171 A. Christodoulakis, E. Heracleous, A. A. Lemonidou and S. Boghosian, *J. Catal.*, 2006, **242**, 16.
172 T. Kim, A. Burrows, C. J. Kiely and I. E. Wachs, *J. Catal.*, 2007, **246**, 370.
173 A. Sharma, G. D. Cody and R. J. Hemley, *Energy Fuels*, 2009, **23**, 5571.